Cyclin Kinase-independent role of p21^{CDKN1A}in the promotion of nascent DNA elongation in unstressed cells

Sabrina F. Mansilla[1], Agustina P. Bertolin[1], Valérie Bergoglio[2*], Marie-Jeanne Pillaire[2*], Marina A. González Besteiro[1], Carlos Luzzani[3], Santiago G. Miriuka[3], Christophe Cazaux[2†], Jean-Sébastien Hoffmann[2] and Vanesa Gottifredi[1#]

[1] Fundación Instituto Leloir-Instituto de Investigaciones Bioquímicas de Buenos Aires. Consejo de Investigaciones Científicas y Técnicas. Avenida Patricias Argentinas 435. 1405. Buenos Aires, Argentina.

[2] Equipe «Labellisée LA LIGUE CONTRE LE CANCER», Laboratoire d'Excellence Toulouse Cancer LABEX TOUCAN - Cancer Research Center of Toulouse, Inserm U1037, CNRS ERL5294 ; University Paul Sabatier, Toulouse, France.

[3] Laboratorio de Investigaciones Aplicadas en Neurociencias (LIAN-CONICET), FLENI, Ruta 9 Km52.5, Belén de Escobar (B1625XAF), Argentina.

*equal contribution

[#] corresponding author:vgottifredi@leloir.org.ar

[†] Deceased August 3, 2015

Running title:

CDK-independent role of p21 in DNA replication

Competing interests

The authors declare that no competing interests exist.

ABSTRACT

The levels of the cyclin-dependent kinase (CDK) inhibitor p21 are low in S phase and insufficient to inhibit CDKs. We show here that endogenous p21, instead of being residual, it is functional and necessary to preserve the genomic stability of unstressed cells. p21depletion slows down nascent DNA elongation, triggers permanent replication defects and promotes the instability of hard-to-replicate genomic regions, namely common fragile sites (CFS). The p21's PCNA interacting region (PIR), and not its CDK binding domain, is needed to prevent the replication defects and the genomic instability caused by p21 depletion. The alternative polymerase kappa is accountable for such defects as they were not observed after simultaneous depletion of both p21 and polymerase kappa. Hence, in CDK-independent manner, endogenous p21 prevents a type of genomic instability which is not triggered by endogenous DNA lesions but by a dysregulation in the DNA polymerase choice during genomic DNA synthesis.

INTRODUCTION

The p21 protein (also known as $p21^{CDKN1A}$ and $p21^{Cip1/Waf1}$), is a member of the family of cyclin-dependent kinase (CDK) inhibitors (CKIs) which has long been known for its ability to consolidate the G1 and G2 arrest after DNA damage caused by genotoxic agents, such as γ irradiation (γ IR)(Brugarolas et al., 1995; Bunz et al., 1998; Deng, Zhang, Harper, Elledge, & Leder, 1995; Dulic, Stein, Far, & Reed, 1998). As p21 has no enzymatic domain, it was not surprising to discover that a robust increase in p21 protein levels is required to achieve efficient CDK inhibition in response to DNA damage (Boulaire, Fotedar, & Fotedar, 2000; Cai & Dynlacht, 1998). Such observations have led to the widely-held assumption that the low amounts of p21 in cycling cells are residual and insufficient to achieve any biological relevant function (Bertolin, Mansilla, & Gottifredi, 2015; Soria & Gottifredi, 2010).

However, p21 levels in cycling cells are not null. Albeit p21 does not efficiently inhibit CDK activity in cycling cells (Cai & Dynlacht, 1998) it could still regulate CDK-independent processes. CDK-independent functions of p21 could rely on its proliferating cell nuclear antigen (PCNA)-interacting region (PIR) located on the C-terminus of p21, which binds the interdomain connecting loop (IDCL) of PCNA with high affinity ((Prives & Gottifredi, 2008) and references there in).However, no role for the p21/PCNA complex formation has been yet described. On the contrary, research has focused only on the biological relevance of disrupting the p21/PCNA interaction.

As DNA polymerases (pols) also bind the IDCL of PCNA through PIR or PIP (PCNA interacting protein) boxes, p21 should be capable of negatively regulating all PCNA-dependent DNA synthesis processes in cells (Moldovan, Pfander, & Jentsch, 2007; Tsanov et al., 2014). In fact, *in vitro* experiments demonstrated that large excess of p21´s PIR inhibits the interaction of PCNA with DNA replication and nucleotide excision repair (NER) factors (for original papers refer to (Prives & Gottifredi, 2008)),impairing

replication- and repair-associated DNA synthesis respectively (see examples in (Cooper, Balajee, & Bohr, 1999; Gottifredi, McKinney, Poyurovsky, & Prives, 2004) (Prives & Gottifredi, 2008)) . However, the amount of p21 used in such experiments were much higher than the maximal p21 levels that can be accumulated in cells, even after genotoxic treatments (discussed in (Prives & Gottifredi, 2008)).The overexpression of p21 to levels in the range of those induced by genotoxins, inhibits neither replication- nor repair- associated DNA synthesis events (Soria, Speroni, Podhajcer, Prives, & Gottifredi, 2008)which are mostly dependent on replicative DNA pols (Burgers, 1998; Soria & Gottifredi, 2010).These data all toghether indicate that in cycling cells, physiological levels of p21 are not capable of inhibiting PCNA-dependent DNA synthesis by replicative DNA pols, even when p21 is induced by external stress.

However, PCNA-dependent synthesis by other DNA pols could be inhibited by endogenous p21. In fact, endogenous p21 levels drop dramatically after ultraviolet irradiation (UV) and Methyl methane sulfonate (MMS) treatments (Soria, Podhajcer, Prives, & Gottifredi, 2006). We have previously shown that p21 downregulation after UV facilitates nascent DNA elongation across UV-damaged DNA templates by enabling the recruitment of alternative (alt) DNA pols to replication factories (Mansilla et al., 2013). Strikingly, UV irradiation couples translesion DNA synthesis (TLS) by alt DNA pols with the activation of the $CRL4^{Cdt2}$ E3 ligase at replisomes (Havens & Walter, 2011; Nishitani et al., 2008; Soria & Gottifredi, 2010). The $CRL4^{Cdt2}$ E3 ligase binds and degrades p21 *only* when it is complexed with chromatin-associated PCNA (Abbas et al., 2008; Havens & Walter, 2011). The list of genotoxic treatments that triggers p21 proteolysis has expanded lately and includes UV, MMS, cisplatin, hypoxia, hypoxia mimicking factors, hydroxyurea (HU), aphidicolin (APH), hydrogen peroxidate, and potassium bromide (Savio et al., 2009). In conclusion, the degradation of endogenous p21 at replication sites in S phase allows full TLS activation or fork-restart when required.

While the above mentioned reports demonstrate the relevance of disrutpting p21-PCNA interaction in cells, no report has ever addressed the relevance of the PCNA-p21 complex in cells. Here we report that endogenous p21 localizes at replication factories through PCNA binding, thereby avoiding DNA polymerase κ (Pol κ) to be recruited at replication factories. Surprisingly, in contradiction with its function as a negative regulator of CDKs, p21 facilitates S phase progression; i.e p21 promotes nascent DNA elongation.The DNA replication defects caused by p21-depletion caused accumulation of replication stress markers, such as γH2AX and 53BP1, instability of common fragile sites and micronuclei (MN) accumulation. Interestinlgy, all the replication defects observed in p21-depleted cells were eliminated when Pol κ was depleted, and were also complemented by a p21 mutant with an intact PCNA binding domain and a disrupted CDK binding site. Collectively, our data demonstrates that, although expressed at low levels in S phase, p21 fine-tunes the dynamics of DNA replication by regulating Pol κ loading to replisomes. Therefore, while the CDKs/p21 interaction is crucial to the cellular response to DNA damage, the PCNA/p21 interaction prevents the accumulation of DNA-damage independent genomic instability in unstressed cycling cells.

RESULTS

p21 localizes to replication factories in cycling cells

The limited amounts of p21 in cycling cells allow CDK-dependent cell cycle progression (Kreis, Sanhaji, Rieger, Louwen, & Yuan, 2014). Indeed, p21 levels in cycling cells are not null and can be detected on EdU positive cells with p21 specific antibodies (Figure 1A and B) as reported recently (Coleman et al., 2015). Remarkably, while p21 levels are at the lowest in S phase (Figure 1- figure supplement 1A -B), they are sufficient to impair TLS-dependent DNA synthesis (Mansilla et al., 2013; Soria & Gottifredi, 2010) if not degraded after UV irradiation (Figure 1- figure supplement 1A -B). Notably, the

function of p21 during unperturbed cell cycle progression remained unknown. A hint of such function was revealed by a Proximity ligation assay (PLA) which revealed a chromatin bound PCNA/p21 interaction in cycling cells. Such complexes resisted a mild extraction with CSK buffer which removes proteins unbound to chromatin (Figure 1C-D). Consistently with our previous findings, the percentage of cells with PLA spots was reduced by UV irradiation and PLA spots were not detected upon p21 depletion (Figure 1C-D). In agreement, endogenous p21 colocalized with PCNA (Figure 1E and 1F) and EdU-labelled replication factories (Figure 1- figure supplement 1C). The colocalization of p21 and GFP-PCNA became more evident following removal of proteins unbound to chromatin (Figure 1- figure supplement 2A). We next evaluated the requirement of the p21 PIR region for p21-PCNA colocalization. To this end, we transfected cells with either p21 or $p21^{PIPMut*}$, bearing an intact or a disrupted PIR, respectively (Mansilla et al., 2013; Soria et al., 2008). The disruption of the CDK-binding site by point mutations in both constructs (Mansilla et al., 2013; Soria et al., 2006; Soria et al., 2008), prevented the arrest outside S phase expected after p21 overexpression (Figure 1-figure supplement 2B -C). Similar to endogenous p21, overexpressed p21 localized to replication factories (Figure 1G and Figure 1- figure supplement 3A -B). However, $p21^{PIPMut*}$lost its ability to form foci at replication factories (Figure 1H and Figure 1-figure supplement 3C), did not colocalize with PCNA (Figure 1-supplement figure 3C) and showed reduced chromatin retention (Figure 1- figure supplement 3D and 3E). Hence, the PIR of p21 is required for the localization of p21 to replication factories in cycling cells.

Endogenous p21 preserves DNA replication homeostasis in cycling cells

On the basis of the localization of p21 to replication factories, we speculated that p21 could regulate the DNA replication dynamics during S phase. To test this hypothesis, we used p21-depleted U2OS osteosarcoma cells (Figure 2A). The number of cells positive for EdU and with PCNA bound to chromatin increased after p21 depletion

(Figure 2B and 2C). An enrichment in PCNA focal distribution corresponding to mid-to-late S phase (Essers et al., 2005; Rey et al., 2009), was found in p21-depleted samples (Figure 2D) which suggested a defect intrinsic to S phase and independent from the G1/S transition.

Therefore, we evaluated DNA replication parameters specific to S phase in p21-depleted U2OS cells by means of the DNA spreading technology. Nascent DNA was labelled with a 10-minutes pulse of CldU (Chlorodeoxyuridine), followed by a 30-minutes pulse of IdU (Iododeoxyuridine). After denaturalization, stretching and labelling with specific antibodies, DNA track lengths were quantified. Surprisingly, p21 loss resulted in reduced track length suggesting that p21 is required for a proper elongation of the replication forks (representative tracks and fields are shown in Figure 2E-F). These findings were confirmed in an additional cellular model, the HCT116 p21 null cells which were compared with the HCT116 p21+/+ counterparts (Figure 2-supplement figure 1A-C). Such findings were unexpected from the perspective of the prevalent notion of p21 as a negative regulator of the cell cycle. Since defective fork elongation is generally coupled to increased origin firing (Blow, Ge, & Jackson, 2011; Pillaire et al., 2007; Techer et al., 2016), we measured the origin frequency as we did in the past (Vallerga, Mansilla, Federico, Bertolin, & Gottifredi, 2015) [number of red-green-red tracks + red tracks only/total fibers] (Figure 2G). Results indicated that p21 depletion upregulated origin firing in the absence of stress (Figure 2H). Thus endogenous p21 is required for the optimal execution of the DNA replication program during unperturbed S phase.

p21 low levels in cycling cells prevent replication stress in the absence of DNA damage

On the basis of the contribution of p21 to unperturbed DNA replication, we tested the effect of p21 depletion on the accumulation of markers of DNA replication stress. The

intensity of γH2AX (Mansilla et al., 2013; Ward & Chen, 2001) increased both in U2OS transfected with p21 siRNA (Figure 3A) and in p21 -/- HCT116 cells (Figure 3- figure supplement 1A-B). Also, the number of cells with more than five 53BP1 foci (Mansilla et al., 2013; Noon & Goodarzi, 2011) (Figure 3B and Figure 3- figure supplement 1C) and the number of cells with RPA foci which reveals long stretches of single stranded DNA (Bergoglio et al., 2013; Oakley & Patrick, 2010) increased when p21 was depleted (Figure 3C).Thus, fork stalling and/or uncoupling events are more frequent in cells attempting to replicate DNA in the absence of p21 than in control samples.

Replication-associated defects could trigger the accumulation of perinuclear DNA or micronuclei (MN) in binucleated cells that have finished karyocinesis (Fenech, 2000). Notably, MN acumulated in cells transiently or permanently depleted from p21 (Figure 3D and Figure 3- figure supplement 1D, respectively). Another marker of genomic instability that is highly sensitive to replication defects is the rearrangements of common fragile sites (CFS) (Le Tallec et al., 2014; Letessier et al., 2011). Because of low origin density, the replication of CFSs is easily compromised by alterations in the replication program (Letessier et al., 2011; Ozeri-Galai, Bester, & Kerem, 2012; Ozeri-Galai et al., 2011). Noteworthy, data in Figure 3E and 3F revealed that p21 depletion caused the accumulation of the FRA7H CFS instability to an extent similar to that caused by low doses of APH, a known inducer of CFS instability (Bergoglio et al., 2013; Sutherland, Parslow, & Baker, 1985). It follows that the depletion of p21 jeopardizes the duplication of hard-to-replicate genomic regions triggering replication-associated genomic instability.

p21 prevents the aberrant use of the alternative DNA polymerase κ during the replication of undamaged DNA

Besides p21, novel negative regulators of alt DNA pols have been recently identified (Bertolin et al., 2015). One of them, USP1, has the ability to remove the ubiquitin

194 moiety from PCNA (Huang et al., 2006; Niimi et al., 2008). Mono-ubiquitinated PCNA
195 interacts with the UBM and UBZ domains of alternative DNA pols favouring their
196 loading to the replisomes (Bienko et al., 2005; P. L. Kannouche & Lehmann, 2004;
197 Plosky et al., 2006). During unperturbed replication, PCNA ubiquitination is limited by
198 USP1 (Huang et al., 2006; Niimi et al., 2008), as evidenced by increased PCNA
199 ubiquitination upon USP1 depletion (Figure 4A and Figure 4B). In constrast, the level of
200 PCNA ubiquitination was not modified when p21 was depleted (Figure 4A). Hence, p21
201 and USP1 regulate the recruitment of alt pols by distinct mechanisms (Figure 4C).
202 Intriguingly, despite such mechanistic differences, both p21 and USP1 depletion
203 caused a similar effect (both in quality and extent) on nascent DNA elongation (Figure
204 4D), origin frequency (Figure 4E), the accumulation of cells with 53BP1 foci (Figure 4F)
205 and the number of binucleated cells with MN (Figure 4G). These results reinforce the
206 function of p21 as a negative regulator of alt DNA pols. Moreover, mechanistically
207 distinct regulators of alt DNA pols are equally required to preserve DNA replication and
208 genomic stability during unperturbed replication.

209 T. Huang and colleagues have previously reported that MN accumulation induced by
210 USP1 depletion depends on Pol κ (Jones, Colnaghi, & Huang, 2012). Therefore, we
211 set to explore the effect of p21 on Pol κ recruitment to DNA replication factories. First,
212 we observed that Pol κ foci were formed only in a modest percentage of control cycling
213 cells (siLuc in Figure 5A-B). However, when p21 was depleted, the percentage of cells
214 with Pol κ foci raised significantly (Figure 5A-B). Second, the interaction of PCNA and
215 GFP-Pol κ in the chromatin fraction increased when p21 was depleted (Figure 5C).
216 Third, using PLA an increase in the number of endogenous PCNA/Pol κ interacting
217 foci was revealed in p21-depleted samples (Figure 5D-E). We hypothesized that an
218 increased recruitment of Pol κ to the replication forks in p21-depleted cell may slow
219 down DNA elongation, triggering fork collapse and/or the generation of under-
220 replicated DNA. To test this hypothesis, Pol κ was down-regulated in p21-depleted

cells (Figure 6A) and different DNA replication parameters were tested. Fourty eight hours after siRNA transfection, Pol κ depletion alone had no effect on most parameters, except from a modest increase in RPA foci formation (Figure 6-supplement figure 1). Such result may be in agreement with the role of Pol κ in the replication of non-B DNA regions such as G4 cuadruplex (Betous et al., 2009). Notably however, the simultaneous elimination of Pol κ and p21 prevented all the phenotypes associated with p21 depletion. Specifically, Pol κ depletion rescued the defective nascent DNA elongation (Figure 6B), the origin frequency (Figure 6C), the percentage of EdU positive cells (Figure 6- figure supplement 1A) and the increased number of cells with chromatin bound-PCNA (Figure 6- figure supplement 1B). Similarly, markers of replication stress such as RPA foci (Figure 6- figure supplement 1C), γH2AX (Figure 6- figure supplement 1D) and 53BP1 foci (Figure 6D) were downregulated after simultaneous depletion of p21 and Pol κ. Similar results were obtained when using a second siRNA specific for Pol κ in U2OS cells (Figure 6- figure supplement 2 A-D) and when employing a different cell line, HCT116 p21 -/- cells (Figure 6-supplement figure 2 E-F).

While MN accumulation was evident when p21 was knocked down, this was not observed after simoultaneous depletion of Pol κ and p21 (Figure 6E). CFS instability modestly increased in Pol κ-depleted cells and more pronouncedly in p21-samples. Remarkably, in the context of p21 elimination, instead of increasing CFS instability Pol κ depletion reverted the instability caused by p21 depletion (Figure 6F-G) Collectively, these findings indicate that the misuse of Pol κ causes multiple alterations in the DNA replication of p21-deficient cells.

The recruitment of the alternative DNA polymerase pol eta (Pol η) to replication factories was also stimulated in the absence of p21 (Figure 6- figure supplement 3A-C). However, in contrast to Pol κ, Pol η depletion did not rescue the replication defects

triggered by p21 depletion (see Figure 6- figure supplement 3D-H). Hence, the parameters of genomic instability explored in this study are predominantly associated with the misuse of Pol κ in p21-depleted samples.

p21 prevents mitotic transmission of DNA damage induced by Pol κ–dependent replicative stress

In addition to the well characterized and direct consequences of DNA replication stress, namely chromosomal breakage and aberrations, it has been shown that a fraction of under-replicated/unresolved genomic loci enter into mitosis. When not accurately processed in M phase, such DNA regions are converted into complex broken-DNA structures that are transmitted to daughter cells (Minocherhomji et al., 2015). In G1 phase such DNA structures are sequestered and shielded in nuclear compartments described as nuclear 53BP1 bodies (Bergoglio et al., 2013; Harrigan et al., 2011; Lukas et al., 2011). We therefore explored whether the altered DNA replication dynamics of p21-depleted cells could lead to the mitotic transmission of DNA damage. We first noticed an increase in the percentage of cells positive for the phosphorylated histone H3 ,a *bona-fide* marker of G2/M transition (Minocherhomji et al., 2015), upon p21 depletion which was again totally reversed by Pol κ depletion (Figure 7A). To confirm the persistence of under-replicated DNA in mitosis, we used previously reported protocols (Federico et al., 2015; Minocherhomji et al., 2015) to quantified 53BP1 body formation in G1 (EdU-negative). We found a significant increase in the number of spontaneous 53BP1 nuclear bodies in G1 in the absence of p21, as hallmark of incomplete DNA replication during the previous cell cycle, which was again dependent on Pol κ (Figure 7B-D). We conclude from these experiments that the choice of Pol κ in the absence of p21 is sufficient to increase the vulnerability of fragile genomic regions by delaying replication completion at these sequences. Such alteration of the DNA replication dynamics appear to be specific to Pol κ since they were not rescued when Pol η was depleted (Figure 7E-F).

The PCNA-binding domain of p21 is necessary and sufficient to prevent the replication defects introduced by Pol κ

Having established that Pol κ triggers replication defects of p21-depleted cells, it was important to determine whether p21 prevents the loading of Pol κ to replication factories and if its ability to interact with PCNA is relevant to such function. We used the p21 mutants described in Figure 1, which are refractory to a siRNA directed to the 3´UTR of p21 (Figure 8A). Lentiviral transduction allowed the expression of p21 and $p21^{PIPMut*}$ in almost all cells (Figure 8B). A fully functional PCNA binding domain in p21 was required to down-modulate Pol κ foci formation to control levels (Figure 8C). In agreement, the fork elongation defects and the excessive origin firing observed in p21-depleted samples were complemented by p21, but not by $p21^{PIPMut*}$ (Figure 8D-E). Additionally, the key role of the PIP domain of p21 was supported by experiments performed in HCT116 p21-/- cells. Such experiments revealed that p21 but not the $p21^{PIPMut*}$ mutant complement the replication defects of cells with a null mutation of the endogenous p21 alleles (Figure 8 F-H). Notably, the accumulation of markers of replication stress and genomic instability in p21-depleted cells was abolished when overexpressing p21, but not $p21^{PIPMut*}$ (Figure 8I-J). Hence, we postulate a key role of the PIP domain of p21 in the preservation of DNA replication homeostasis.

p21 preserves the genomic stability of primary cells

Given that our results indicate a novel antioncogenic role of p21 in the promotion of DNA replication it was important to determine wheather this phenotype was not limited to cancer cells. To address such question we used primary cells from two independent sources: a) human foreskin fibroblast (HFF) and b) mesenchyimal stem cells isolated from umbilical cord (MSC). As showed in Figure 9A and B, transfection of p21 siRNA efficiently depleted p21 from both cell types. p21 elimination caused a reduction in the elongation of nascent DNA (Figure 9A-C), which was accompanied with an increase in

origin firing (Figure 9D). In turn, such alteration in DNA replication parameters correlated with the accumulation of cells with 53BP1 foci (Figure 9E-F) and micronuclei (Figure 9 G-I). Hence, we postulate that p21 regulates protein-complex formation at the replisomes, promoting the choice of the most adequate polymerase and therefore protecting DNA replication homeostasis. Such novel function of p21 depends exclusively on its ability to interact with PCNA and is needed at every S phase to ensure the accurate finalization of DNA replication (see model in Figure 10).

DISCUSSION

We describe a biologically relevant contribution of the interaction of p21 and PCNA in cells. We show that such interaction improves DNA replication dynamics since it is required to ensure the best rate of nascent DNA elongation. By promoting accurate DNA polymerase choice at the replisome, p21 acts as a tumor suppressor chronically at each duplication cycle, in the absence of exogenous sources of DNA damage.

A novel function of p21 in the fine-tuning of DNA replication dynamics

An important implication of our findings is that the idea that p21 acts excusively as a negative regulator of the cell cycle through the inhibition of cycling kinases (Warfel & El-Deiry, 2013) is simplified, incomplete and limited to specific DNA-damaging scenarios. The results presented herein conclusively show that p21 is more often a positive rather than a negative regulator of the cell cycle, as its contribution is required at every S phase. Remarkably, such contribution relies exclusively on the p21/PCNA interaction.

Previous work indicates that p21 can displace alt DNA pols from replicating DNA. First, Z. Livneh and colleagues showed that p21 impairs TLS events on transfected plasmids (Avkin et al., 2006). Second, the low levels of p21 in cycling cells must be eliminated to promote nascent DNA elongation across UV damage templates by alt DNA pols (Mansilla et al., 2013). Third, endogenous p21 delays the recruitment of alt DNA pols to

UV-damaged replication factories in a manner that correlates with the extent of p21 degradation (Mansilla et al., 2013; Soria et al., 2008). Fourth, the PCNA-binding domain of p21 is required to inhibit TLS activation (Avkin et al., 2006; Mansilla et al., 2013; Soria et al., 2008). It follows that alt DNA pols might be selectively sensitive to p21 levels which are insufficient to inhibit CDKs (Soria & Gottifredi, 2010). Such a difference in the levels of p21 required to inhibit different cellular processes indicates that p21 is locally concentrated at, and/or has very high affinity for PCNA (Soria & Gottifredi, 2010). Both replicative and alt DNA pols bind the IDCL of PCNA through PIR or PIP (PCNA interacting protein) regions (Bertolin et al., 2015; Moldovan et al., 2007). The PIR of p21 binds PCNA strongly, so that p21 is capable of disrupting the weaker interactions between PCNA and alt DNA pols (Hishiki et al., 2009; Mansilla et al., 2013; Tsanov et al., 2014) without affecting replicative DNA pols which have multiple PIP domains(Soria & Gottifredi, 2010; Soria et al., 2008). Such difference may relate to the fact that replicative DNA pols utilize multiple domains and different sites to interact with PCNA (Johansson, Garg, & Burgers, 2004; Moldovan et al., 2007).

There is a tight cross-regulation of PIP box-containing proteins at replication forks which is not yet completely understood. On the one hand, it has been demonstrated that proteins with strong PIP boxes such as p21 can remove alt pols such as Pol κ from replication factories (this report and (Tsanov et al., 2014)).On the other hand, this and previous reports (Jones et al., 2012; Pillaire et al., 2007) suggest that the alt Pol κ can displace replicative pols from replisomes. Conversely however, p21-PCNA interaction in S phase does not impair genomic DNA synthesis (Soria et al., 2008) suggesting that p21 cannot displace replicative DNA pols from the replisome. Hence, some yet unknown factors/events need to be identified to understand the hierarchy of PCNA partners at forks. Moreover, variables such as the sequence of the DNA which is being replicated and the average retention time of a PCNA partner at different regions of the chromatin might have a role in such a puzzling cross-regulation among PCNA partners.

353 We have shown that Pol κ is required for checkpoint activation at stalled forks (Betous
354 et al., 2013) and during the replication of repetitive sequences (Hile, Wang, Lee, &
355 Eckert, 2012) or naturally occurring non-B DNA structures (Betous et al., 2009). In
356 agreement, Pol κ depletion affected the CFS expression and RPA accumulation in our
357 experimental settings. It is therefore possible that certain DNA regions may benefit
358 from Pol κ-dependent DNA synthesis (Betous et al., 2009) while others it might
359 require active displacement of Pol κ by p21. If that is the case, p21 may prevent Pol κ
360 recruitment to specific regions of the genome while prompt p21 degradation by
361 $CLR4^{Cdt2}$ might rapidly allow Pol κ binding to others. Such p21 function could be
362 executed either by promoting the dissociation of Pol κ from replisomes or by preventing
363 its recruitment to DNA regions that must be necessarily copied by replicative DNA pols
364 (such as for example B-regions in the exonic DNA).

365 **The complex regulation of Pol κ by p21**

366 The PIR domain of p21 prevents the recruitment of Pol η, Pol ι, Pol κ and Rev1 to UV-
367 damaged replication factories (Bertolin et al., 2015; Mansilla et al., 2013). Hence, it is
368 unlikely that during unperturbed replication p21 would act as a specific inhibitor of Pol
369 κ. The same is valid for USP1 because the modulation of PCNA ubiquitination should
370 regulate all alt DNA pols (Huang & D'Andrea, 2006; Jones et al., 2012). Hence, p21
371 and USP1 depletion may result in increased loading of all alt DNA pols to undamaged
372 DNA. In fact, others have reported increased spontaneous mutation frequency in the
373 hypoxanthine phosphoribosyl transferase (hprt) locus of p21-/- cells, (McDonald, Wu,
374 Waldman, & El-Deiry, 1996). Such defects might depend on the unleashed activity of
375 alt DNA pols other than Pol κ (Yang & Woodgate, 2007). Notwithstanding this, the
376 phenotypes described herein are intimately associated with processive DNA synthesis
377 events, and Pol κ is a very processive alt DNA pol (the most processive in the Y family)
378 (Ohashi et al., 2000; Zhang et al., 2000). Because Polκ is less processive than

379 replicative DNA pols (McCulloch & Kunkel, 2008; Ohashi et al., 2000), the coupling of a
380 replicative DNA pol and Pol κ at a single replisome may most likely generate
381 asynchronic speed in both DNA strands. In turn, this may cause the transient
382 accumulation of ssDNA in one strand (see Figure 3C). In fact, low doses of APH, which
383 are known to disrupt the DNA pol homeostasis during DNA replication, cause similar
384 levels of CFS expression as p21 depletion (see Figure 3E). Hence, the local
385 degradation of p21 by $CLR4^{CDT2}$ may maintain the most efficient DNA elongation speed
386 by allowing the rapid and dynamic exchange of replicative DNA pols for Pol κ. In fact, a
387 minor shift in the timing of $CLR4^{CDT2}$-dependent p21 degradation is sufficient to
388 accumulate cells in S phase (Coleman et al., 2015). Notably, the elimination of not only
389 p21 but also USP1 (Jones et al., 2012) increases the use of Pol κ during undamaged
390 DNA replication, suggesting that the slightest modulation of Pol κ activity perturbs the
391 DNA replication dynamics. In agreement, the expression of a Pol κ mutant with
392 increased affinity for PCNA and the overexpression of Pol κ generate genomic
393 instability and tumor formation (Bavoux, Hoffmann, & Cazaux, 2005; Bavoux,
394 Leopoldino, et al., 2005; Bergoglio, Bavoux, Verbiest, Hoffmann, & Cazaux, 2002;
395 Hoffmann & Cazaux, 2010; J et al., 2001; Jones et al., 2012).

396 **The biological consequences of excessive genomic DNA synthesis by Pol κ**

397 It is relevant to mention that the p21 knock out mice develop spontaneous tumors at 16
398 months (Martin-Caballero, Flores, Garcia-Palencia, & Serrano, 2001), suggesting that
399 modest but accumulative defects eventually trigger oncogenic transformation. Such
400 observation highlights a role of p21 in the face of chronic, rather than acute stress and
401 may correlate with the multiple defects in DNA replication revealed when depleting p21
402 from primary cells (Figure 9). While p21 is a negative regulator of TLS, its role in
403 undamaged DNA replication (revealed in this manuscript) is most possibly *unrelated* to
404 TLS inhibition. In fact, if p21 depletion caused the accumulation of DNA lesions, the

elimination of an alt polymerase should: a) aggravate the defect (if the alt pol is essential to promote DNA replication across the replication barrier) or b) not alter such defect (if the replication across such barrier is also achieved by another alt polymerase) (Bertolin et al., 2015). As our data shows that the elimination of Pol κ promotes DNA replication, it does not support a model in which p21 depletion generates substrates (DNA lesions) for alt pols. On the contrary, it suggests that undamaged DNA is being misused by the alternative polymerase pol κ as a replication template . Hence, the contribution of p21 to unperturbed-DNA replication is most probably related to the control of DNA synthesis events on undamaged templates. In such scenario, the colocalization of the p21-CLR4^{cdt2} complex at replication forks may be crucial to control the composition of the active replisome, allowing the selection of the most adequate polymerase “on the go”. Such dynamic regulation would favour the most effective DNA replication speed allowing the timely activation of late and hard-to-replicate genomic regions. The coupling of p21 with ongoing replisomes may also favor other p21 functions as homologous recombination (HR) events. While such p21 function has been linked to CDK inhibition (Mauro et al., 2012), it is still possible that the loading of p21 to PCNA serves to orchestrate multiple transactions at the elongating DNA. While more work is required to reveal yet hidden cross-regulations among members of the replisome, our work unveils a novel tumor suppressor function of p21 dependent on its ability to interact with PCNA. Such role of p21 is central for genome maintenance in the absence of DNA damage at every S phase and which might be key to prevent spontaneous oncogenic events.

Materials and Methods

Cell culture and reagents: All cell lines were received from reliable sources, either public repositories or directly, from the laboratory that generated them. They were never freezed at passage higher than 8. U2OS (source: ATCC), and HCT116 p21+/+ and HCT116 p21-/- (gifts from B. Vogelstein-Johns Hopkins University, Baltimore) were

received directly from ATCC and Johns Hopkins University respectively. Samples were minimally amplified and freezed after reception and were used for limited passages after thawing of those primary stocks. We have verified the identity of the cell lines in terms of the pathways which are key for this study. We have verified the p53 and p21 status by RT-PCR. The three cell lines are positive for p53 and only U2OS and HCT 116 p21+/´+ were positive for p21, while HCT 116 p21-/- was not. None of the used cell lines were in the list of commonly misidentified cell lines maintained by the International Cell Line Authentication Committee (Capes-Davis A et al, 2010) updated in http://iclac.org/databases/cross-contaminations/). Samples were grown in Dulbecco's modified Eagle's medium (Invitrogen) with 10% fetal calf serum in a 5% CO2 atmosphere. Samples are routinely tested for mycoplasma by PCR every two weeks.

Umbilical cord mesenchymal stem cells (UC-MSC) were isolated from Wharton jelly tissues. Small pieces of the umbilical cord, excluding the major vessels, were layered onto plastic culture plates and cultured in D-MEM supplemented with 10% SFB and penicillin-streptomycin. After 14 days, cells started to emerge from the tissue pieces. When plates were almost confluent, umbilical cord pieces were removed and cells trypsinized and frozen. Multilineage differentiation potential of UC-MSC was assessed using StemPro Adipogenesis, Osteogenesis or Chondrogenesis Kit (Life Technologies, US) as per instruction of the manufacturer. Human Foreskin Fibroblasts (HFF) were obtained under informed consent from his parents from the foreskin of a three-year old boy undergoing a scheduled surgery. HFF were obtained using a similar protocol to the one used with UC-MSC. Both cell lines were grown in DMEM supplemented with 10% FBS and antibiotics up to a 15 passage. All isolations of primary cells were approved by FLENI Ethic Committee after reviewing the research protocol (Luzzani et al., 2015).

The HFF (Human Foreskin Fibroblasts) were analyzed by karyotyping to assess genomic integrity after 10 passages. Experiments were performed using cells up to passage number 15 to prevent the occurrence of abnormalities. In addition, cells´ surface markers are periodically analized by flow citometry. MSC line were used up to

passage number 10 to prevent genomic aberrations and lost of stem cells´ properties. MSC surface markers expression profile and their differentiation potential were periodically analized by flow citometry and by chondregic, adipogenic and osteogenic differentiation, respectively. MSC immunomodulatory properties were also assessed by CFSE lymphocyte proliferation assay. All cell lines were weekly analyzed for mycoplasm contamination by PCR. Transfections of siRNAs were performed using Lipofectamine® RNAiMAX (Thermofisher) and Jet Prime (Polyplus) was used when delivering both siRNAs and plasmid expression vectors.

siRNAs, vector expression plasmids and lentiviral infection. GFP-Pol η and GFP-Pol κ were gifts from Dr. A. Lehmann (P. Kannouche et al., 2001). GFP-PCNA was kindly provided by Dr M. C. Cardoso (Max Delbrück Center for Molecular Medicine, Berlin, Germany) (Leonhardt et al., 2000) siRNAs were purchased from Dharmacon:

siRNA p21 3'UTR:GGAACAAGGAGUCAGACAU;

siRNAUSP1:UCGGCAAUACUUGCUAUCUUA (Jones et al., 2012);

siRNA Pol κ1: AAGAUUAUGAAGCCCAUCCAA (Vallerga et al., 2015);

siRNA Pol κ2: AACCUCUAGAAAUGUCUCAUA (Jones et al., 2012)

siRNA Pol η: CUGGUUGUGAGCAUUCGUGUA (Vallerga et al., 2015).

In this work, we used a previously described p21 expression vectors (CS2-p21) and generated the $p21^{PIPMut*}$ (CS2-p21 with the M147 to A, D149 to A and F150 to A mutations which were showed to disrupt the PCNA/p21 interaction (Gulbis, Kelman, Hurwitz, O'Donnell, & Kuriyan, 1996; Mansilla et al., 2013)) Both the p21 and the $p21^{PIPMut*}$ vectors bear three point mutations in its CDK binding domain (W49 to R,F51 to S and D52 to A) which disrupt CDK2/p21 interaction (Gulbis et al., 1996; Mansilla et al., 2013). Primers used to generate p21 mutations were described and validated in

485 our previous work (Mansilla et al., 2013) and both mutations were characterized
486 previously (Gulbis et al., 1996).
487 p21 and p21^{PIPMut*} were cloned into the lentiviral transfer plasmid pLenti CMV/TO Puro
488 (Plasmid #17482, Addgene, 3rd generation) using BamHI and XbaI. Packaging and
489 envelope 2nd generation vectors used were psPAX2 and PMD2.G respectively.
490 Lentiviral particles were obtained by transfecting with Jet prime Hek293T cells in 60mm
491 dishes in a 5:5:1 ratio (pLenti: psPAX2:PMD2). 48hs after transfection lentiviral
492 particles were collected from the supernatant of Hek293T cells, centrifuged, filtered
493 with a 0.45um filter and stored at -80°C. Lentiviral preparations were slowly thawed and
494 used to infect U2OS cells in 24/12 well dishes in the presence of 8µg/ml of polybrene.
495 Infection efficiency was approximately 90% (Figure 7B).
496
497 **Immunostaining and fluorescence detection.** For the quantification and
498 inmunodetection of specialized GFP tagged Pol κ and Pol η, 53BP1 and γH2AX
499 respectively, cells were fixed in 2% paraformaldehyde (PFA)/2% sucrose and
500 permeablized with 0.1% Triton X-100 in phosphate buffered saline (PBS) as described
501 previously (Mansilla et al., 2013). For the detection of chromatin bound proteins ice
502 cold 0.5% Triton CSK buffer was used (10 mM Pipes, pH 7.5, 100 mM NaCl, 300 mM
503 sucrose, 3 mM MgCl2). Proteins were preextracted 1 minute or 5 minutes when
504 detecting p21 or RPA/PCNA respectively. EdU was detected following manufacturer's
505 instructions (Click-iT EdU kit– C10338 Invitrogen). Blocking was performed overnight in
506 PBS 2% donkey serum (Sigma). Coverslips were incubated for 1 h in primary
507 antibodies: 53BP1(Santa Cruz), γH2AX (EMD Millipore), p21 (c-19 Santa Cruz), RPA
508 (NA18 EMD Millipore), PCNA (Abcam), pH3 (ser10 Millipore). Secondary anti-
509 mouse/rabbit-conjugated Cy2/Cy3 antibodies were from Jackson Immuno Research
510 and anti-rabbit alexa 488 from Invitrogen. GFP-tagged specialized Y polymerases and
511 GFP-PCNA were detected by GFP autofluorescence. Nuclei were stained with DAPI

512 (SIGMA). Images were obtained with a Zeiss Axioplan confocal microscope or a Zeiss
513 Axio Imager A2.

514 **Protein Analysis.** For Western blot analysis, samples were lysed in Laemmli buffer.
515 Antibodies used were anti-p21 (c-19; Santa Cruz Biotechnology) anti-polη (H-300;
516 Santa Cruz Biotechnology), , anti-KU70 (A9; Santa Cruz Biotechnology), and anti-GFP
517 (Santa Cruz Biotechnology). Secondary antibodies (Sigma) and ECL detection
518 (Amersham GE Healthcare) were used according to the manufacturers' instructions.
519 Western blot images were taken with Image QuantLAS4000 (GE Healthcare), which
520 allows capture and quantification of images within a linear range. These images were
521 then quantified with the ImageJ software when indicated.

522 **DNA Fiber spreading.** DNA fibers were analysed using a protocol previously used by
523 us (Mansilla et al., 2013) with a minor change in the time of labelling. Exponentially
524 growing cells were pulse labeled with CldU (20 μM) for 10 min, washed twice,and
525 incubated with IdU(200 μM) for additional 30 min. Cells were trypsinized and lysed with
526 6 μl of 0.5% SDS, 200mM Tris–HCL (pH 7.4) and 50mM EDTA buffer onto clean glass
527 slides, which were tilted, allowing DNA to unwind. Samples were fixed in 3:1
528 methanol/acetic acid and denatured with HCL (2.5 N) for 1 h, blocked in PBS
529 5%Bovine serum albumin (BSA) for 15 min and incubated with the mouse anti-BrdU
530 (Becton Dickinson) to detect IdU, donkey anti-mouse Cy3-conjugated secondary
531 antibody (Jackson Immuno Research), rat anti-BrdU (Accurate Chemicals) to detect
532 CldU and donkey antirat Alexa 488 secondary antibody (Invitrogen). Slides were
533 mounted with Mowiol 488 (Calbiochem), and DNA fibers were visualized using a Zeiss
534 Axioplanconfocal microscope. Images were analysed using Zeiss LSM Image Browser
535 software and Image J software. Each data set is derived from measurement of 85-100
536 fibers.

Chromatin Immunoprecipitation of PCNA.Chromatin immunoprecipitations were performed as described in (Soria et al., 2008). U2OS cells were plated in 100 mm culture dishes, transfected with either Luc or p21 siRNA and 24 hs later transfected with GFP-Pol Kappa. Cells were rinsed twice with cold PBS and then extracted with 5 mL of CSK buffer (250 mM sucrose, 25 mM KCl, 10 mM HEPES at pH 8.0, 1 mM EGTA, and 1 mM MgCl2) for 10 min in ice. The CSK-extracted cells were fixed with 1% formaldehyde in PBS (4.5 mL) for 12 min. Then, 0.5 mL of 1 M glycine was added for 5 min to quench the cross-linking reaction. The cross-linked nuclei were rinsed with PBS and then lysed in 750 µL of IP lysis buffer (10 mM Tris·HCl at pH 7.5, 25mM FNa, 20 mM NaCl, 1% Nonidet P-40, 1% Na-Deoxicholate, and 0.1% SDS) freshly supplemented with protease and phosphatase inhibitors. Lysates were scraped from the plates and transferred into 1.5-mL Microfuge tubes. Samples were sonicated (Bioruptor Sonication System, Diagenode) and clarified by centrifugation at 12,000 × g for 30 min at 4ºC. PCNA was immunoprecipitated overnight at 4 °C with 5 µL of monoclonal PCNA antibody (PC-10 AC; Santa Cruz Biotechnology). Samples were washed, lysed in Laemmli buffer and heated at 99ºC for 30 minutes to revert the crosslink, and resolved in SDS/PAGE for Western blot analysis.

Proximity Ligation Assay (PLA). U2OS cells were seeded onto 22mm x 22mm coverslips in 6 well plates. 24hs later cells were pre-extracted with ice cold CSK buffer (PIPES 10mM, NaCl 100mM, sucrose 300mM, MgCl2 3mM,triton 0.5%) for 2 minutes and fixed with PFA 4% for 10 minutes. After pre-extraction and fixation, interaction between endogenous p21 and PCNA was detected following manufacturer's instructions Duolink® In Situ – Fluorescence (SIGMA). Briefly PLA's principle is based on detecting proteins in close proximity (30-40nm) by using different species of primary antibodies. A pair of oligonucleotide (PLA probes) detect the primary antibodies bound the proteins of interest and generates a signal only when the two PLA probes have bound in close proximity, meaning that the samples are localized in close proximity.

564 The signal from each detected pair of PLA probes is visualized as an individual
565 fluorescent spot. These PLA signals can be quantified (counted) and assigned to a
566 specific subcellular location based on microscopy images. Images were obtained with a
567 Zeiss Axioplan confocal microscope and PLA spots were counted using Image J
568 software, cells were counted as positive when more than 3 PLA spots were detected.
569 When analyzing pol κ/PCNA interaction a pol κ "home made" monoclonal antibody
570 from mice purified by Biotem (clone n°16A7-3A11) and PCNA rabbit polyclonal (Abcam
571 ref ab18197) were used. For the quantification of number of foci per nuclei the Cell
572 Profiler program was used to analyze more than 1000 nuclei.

573 **Quantitative Real-Time PCR.** After transfection with the indicated siRNAs, cells were
574 lysed and total RNA was extracted using TRIzol Reagent (Invitrogen). Total RNA (1µg)
575 was used as a template for cDNA synthesis utilizing an ImProm-II Reverse
576 Transcription System (Promega) and oligo-dT as a primer. Quantitative real-time PCR
577 was performed using the MX3005P quantitative PCR instrument (Stratagene) with Taq
578 DNA poly-merase (Invitrogen) and SyberGreen and ROX as reference dyes
579 (Invitrogen). Samples were normalized using GAPDH primers. Both target gene and
580 GAPDH amplification reactions approached 100% efficiency as determined by
581 standard curves. Three independent biological samples were analyzed, and one
582 representative set of results is shown. Primer sequences were as follows: USP1
583 (Forward): 5'- GGACGCGTTGCTTGGAATGT-3' (Reverse) 5'-
584 TGCCCATCTCAGGGTCTTCA-3'. GADPH: (Forward) 5'-
585 AGCCTCCCGCTTCGCTCTCT-3' (Reverse) 5'-GAGCGATGTGGCTCGGCTGG-3'
586 (Vallerga et al., 2015).

587 **MN assay.** Transfected cells were replated at low density. 24 hours after replating
588 cytochalasine B (4.5 ug/ml-Sigma) was added to the media and 40 h later cells were
589 washed 1 min with hypotonic buffer (KCl 0.0075 M) diluted 1/10 from stock solution in

PBS 1X, twice with PBS 1X and fixed with PFA/sucrose 2% for 20 min. DAPI staining served to visualize cells nuclei. 300 binucleated cells were analyzed.

FISH analysis. Cells were treated with 0.1 µg/ml colcemid (Gibco) for 3 h. Cells were trypsinized for 1 minute trying to take off only the mitotic cells. After centrifugation cell pellets were resuspended in hypotonic solution (0.075 M KCl) and incubated for 15 min at 37°C. Samples were then fixed in a methanol/acetic acid solution (3:1), washed three times in the fixative solution and dropped on slides to obtain spread chromosomes. Metaphase slides were incubated with Rnase (10 µg/ml in 2× SSC) for 1 h at 37°C followed by dehydration in successive ethanol baths (70, 85, and 100%). The RP 11 36B6 BAC (corresponding to FRA7H locus) was labeled by nick translation (Abbott) with green dUTP (Vysis Spectrum) and ethanol precipitated with human Cot-1 DNA (Roche) overnight at -20°C. Precipitated DNA was incubated for 1 h at 37°C in hybridization mix. The probe was denatured for 8 min at 70°C and applied to denatured metaphases. Samples were incubated over night at 37°C and, after washing (1X SSC, 5 min at 72°C and SCC 1X 5 min at RT) and mounted in VECTASHIELD Antifade Mounting Medium with DAPI. The images were acquired by using an inverted wide-field Zeiss Axio Observer Z1 microscope fitted with a x63 oil NA 1.4 objective and a Axiocam MRm CDD camera.

Statistical Analysis. Frequency distributions of DNA track length were determined with GraphPad Prism 5 software. In non-Gaussian distributions, Mann–Whitney and Kruskal–Wallis tests were used for statistical analyses when comparing two and more than three variables, respectively. Other statistical analysis were performed with GraphPad in Stat software using the Student's t test and the one-way ANOVA test when applicable.

Acknowledgmentsand Financial Disclosure

We would like to thank Professors AR Lehmann (University of Sussex) and Maria Cristina Cardoso (Max Delbrück Center for Molecular Medicine, Berlin, Germany) for the gift of reagents.This work was supported by grants from National Institute of Health (R03 TW008924) and the Agencia Nacional de Promoción Científica y Tecnológica (ANPCyT) to VG and from La Ligue Nationale contre le Cancer (Equipe Labellisée) and the Laboratoire d'Excellence Toulouse Cancer LABEX TOUCAN grant (Integrative analysis of resistance in hematological cancers) to JSH. VG and MGB are researchers from the National Council of Scientific and Technological Research (CONICET). SFM and APB are supported by fellowships from CONICET.SFM was also supported by a short-term fellowship from The Journal of Cell Science to visit the JSH laboratory. Christophe Casaux is listed as an author as he contributed actively to this proyect and sadly passed away before sumbmitting the manuscript.

Authors contribution

SFM, AB, VB, MJP performed research

SFM, AB, MJP, VB, JSH and VG acquired and analysed data

MGB, CL, SGM and CC contributed with new analytical tools

MGB; CL, SGM generated critical new reagents

CC and VG designed the project

VG wrote the paper and SFM, MGB, AB and JSH edited it

MJP, VB, CL, SGM revised the final draft critically for important intellectual content

SFM, AB; MJP, VB, MGB, CL, SGM, JSH and VG approved the final version to be published

References

Abbas, T., Sivaprasad, U., Terai, K., Amador, V., Pagano, M., & Dutta, A. (2008). PCNA-dependent regulation of p21 ubiquitylation and degradation via the

642 CRL4Cdt2 ubiquitin ligase complex. *Genes Dev, 22*(18), 2496-2506. doi:
643 10.1101/gad.1676108
644 Avkin, S., Sevilya, Z., Toube, L., Geacintov, N., Chaney, S. G., Oren, M., & Livneh, Z.
645 (2006). p53 and p21 regulate error-prone DNA repair to yield a lower mutation
646 load. *Mol Cell, 22*(3), 407-413. doi: 10.1016/j.molcel.2006.03.022
647 Bavoux, C., Hoffmann, J. S., & Cazaux, C. (2005). Adaptation to DNA damage and
648 stimulation of genetic instability: the double-edged sword mammalian DNA
649 polymerase kappa. *Biochimie, 87*(7), 637-646. doi:
650 10.1016/j.biochi.2005.02.007
651 Bavoux, C., Leopoldino, A. M., Bergoglio, V., J, O. W., Ogi, T., Bieth, A., . . . Cazaux,
652 C. (2005). Up-regulation of the error-prone DNA polymerase {kappa} promotes
653 pleiotropic genetic alterations and tumorigenesis. *Cancer Res, 65*(1), 325-330.
654 Bergoglio, V., Bavoux, C., Verbiest, V., Hoffmann, J. S., & Cazaux, C. (2002).
655 Localisation of human DNA polymerase kappa to replication foci. *J Cell Sci,*
656 *115*(Pt 23), 4413-4418.
657 Bergoglio, V., Boyer, A. S., Walsh, E., Naim, V., Legube, G., Lee, M. Y., . . . Hoffmann,
658 J. S. (2013). DNA synthesis by Pol eta promotes fragile site stability by
659 preventing under-replicated DNA in mitosis. *J Cell Biol, 201*(3), 395-408. doi:
660 10.1083/jcb.201207066
661 Bertolin, A. P., Mansilla, S. F., & Gottifredi, V. (2015). The identification of translesion
662 DNA synthesis regulators: Inhibitors in the spotlight. *DNA Repair (Amst), 32*,
663 158-164. doi: 10.1016/j.dnarep.2015.04.027
664 Betous, R., Pillaire, M. J., Pierini, L., van der Laan, S., Recolin, B., Ohl-Seguy, E., . . .
665 Hoffmann, J. S. (2013). DNA polymerase kappa-dependent DNA synthesis at
666 stalled replication forks is important for CHK1 activation. *EMBO J, 32*(15), 2172-
667 2185. doi: 10.1038/emboj.2013.148
668 Betous, R., Rey, L., Wang, G., Pillaire, M. J., Puget, N., Selves, J., . . . Hoffmann, J. S.
669 (2009). Role of TLS DNA polymerases eta and kappa in processing naturally
670 occurring structured DNA in human cells. *Mol Carcinog, 48*(4), 369-378. doi:
671 10.1002/mc.20509
672 Bienko, M., Green, C. M., Crosetto, N., Rudolf, F., Zapart, G., Coull, B., . . . Dikic, I.
673 (2005). Ubiquitin-binding domains in Y-family polymerases regulate translesion
674 synthesis. *Science, 310*(5755), 1821-1824. doi: 10.1126/science.1120615
675 Blow, J. J., Ge, X. Q., & Jackson, D. A. (2011). How dormant origins promote complete
676 genome replication. *Trends Biochem Sci, 36*(8), 405-414. doi:
677 10.1016/j.tibs.2011.05.002

678 Boulaire, J., Fotedar, A., & Fotedar, R. (2000). The functions of the cdk-cyclin kinase
679 inhibitor p21WAF1. *Pathol Biol (Paris), 48*(3), 190-202.
680 Brugarolas, J., Chandrasekaran, C., Gordon, J. I., Beach, D., Jacks, T., & Hannon, G.
681 J. (1995). Radiation-induced cell cycle arrest compromised by p21 deficiency.
682 *Nature, 377*(6549), 552-557. doi: 10.1038/377552a0
683 Bunz, F., Dutriaux, A., Lengauer, C., Waldman, T., Zhou, S., Brown, J. P., . . .
684 Vogelstein, B. (1998). Requirement for p53 and p21 to sustain G2 arrest after
685 DNA damage. *Science, 282*(5393), 1497-1501.
686 Burgers, P. M. (1998). Eukaryotic DNA polymerases in DNA replication and DNA
687 repair. *Chromosoma, 107*(4), 218-227.
688 Cai, K., & Dynlacht, B. D. (1998). Activity and nature of p21(WAF1) complexes during
689 the cell cycle. *Proc Natl Acad Sci U S A, 95*(21), 12254-12259.
690 Capes-Davis A, Theodosopoulos G, Atkin I, Drexler HG, Kohara A, Macleod RA,
691 Masters JR, Nakamura Y, Reid YA, Reddel RR, Freshney RI (2010) Check your
692 cultures! A list of cross-contaminated or misidentified cell lines. Int J Cancer
693 127(1): 1-8.
694 Coleman, K. E., Grant, G. D., Haggerty, R. A., Brantley, K., Shibata, E., Workman, B.
695 D., . . . Cook, J. G. (2015). Sequential replication-coupled destruction at G1/S
696 ensures genome stability. *Genes Dev, 29*(16), 1734-1746. doi:
697 10.1101/gad.263731.115
698 Cooper, M. P., Balajee, A. S., & Bohr, V. A. (1999). The C-terminal domain of p21
699 inhibits nucleotide excision repair In vitro and In vivo. *Mol Biol Cell, 10*(7), 2119-
700 2129.
701 Deng, C., Zhang, P., Harper, J. W., Elledge, S. J., & Leder, P. (1995). Mice lacking
702 p21CIP1/WAF1 undergo normal development, but are defective in G1
703 checkpoint control. *Cell, 82*(4), 675-684.
704 Dulic, V., Stein, G. H., Far, D. F., & Reed, S. I. (1998). Nuclear accumulation of
705 p21Cip1 at the onset of mitosis: a role at the G2/M-phase transition. *Mol Cell*
706 *Biol, 18*(1), 546-557.
707 Essers, J., Theil, A. F., Baldeyron, C., van Cappellen, W. A., Houtsmuller, A. B.,
708 Kanaar, R., & Vermeulen, W. (2005). Nuclear dynamics of PCNA in DNA
709 replication and repair. *Mol Cell Biol, 25*(21), 9350-9359. doi:
710 10.1128/MCB.25.21.9350-9359.2005
711 Federico, M. B., Vallerga, M. B., Radl, A., Paviolo, N., Bocco, J. L., Di Giorgio, M., . . .
712 Gottifredi, V. (2015). Chromosomal integrity after UV irradiation relays on
713 FANCD2-mediated repair of double strand breaks. *PLoS Genetics, minor*
714 *revision PLoS Genetics*.

715 Fenech, M. (2000). The in vitro micronucleus technique. *Mutat Res, 455*(1-2), 81-95.
716 Gottifredi, V., McKinney, K., Poyurovsky, M. V., & Prives, C. (2004). Decreased p21
717 levels are required for efficient restart of DNA synthesis after S phase block. *J*
718 *Biol Chem, 279*(7), 5802-5810. doi: 10.1074/jbc.M310373200
719 Gulbis, J. M., Kelman, Z., Hurwitz, J., O'Donnell, M., & Kuriyan, J. (1996). Structure of
720 the C-terminal region of p21(WAF1/CIP1) complexed with human PCNA. *Cell,*
721 *87*(2), 297-306.
722 Harrigan, J. A., Belotserkovskaya, R., Coates, J., Dimitrova, D. S., Polo, S. E.,
723 Bradshaw, C. R., . . . Jackson, S. P. (2011). Replication stress induces 53BP1-
724 containing OPT domains in G1 cells. *J Cell Biol, 193*(1), 97-108. doi:
725 10.1083/jcb.201011083
726 Havens, C. G., & Walter, J. C. (2011). Mechanism of CRL4(Cdt2), a PCNA-dependent
727 E3 ubiquitin ligase. *Genes Dev, 25*(15), 1568-1582. doi: 10.1101/gad.2068611
728 Hile, S. E., Wang, X., Lee, M. Y., & Eckert, K. A. (2012). Beyond translesion synthesis:
729 polymerase kappa fidelity as a potential determinant of microsatellite stability.
730 *Nucleic Acids Res, 40*(4), 1636-1647. doi: 10.1093/nar/gkr889
731 Hishiki, A., Hashimoto, H., Hanafusa, T., Kamei, K., Ohashi, E., Shimizu, T., . . . Sato,
732 M. (2009). Structural basis for novel interactions between human translesion
733 synthesis polymerases and proliferating cell nuclear antigen. *J Biol Chem,*
734 *284*(16), 10552-10560. doi: 10.1074/jbc.M809745200
735 Hoffmann, J. S., & Cazaux, C. (2010). Aberrant expression of alternative DNA
736 polymerases: a source of mutator phenotype as well as replicative stress in
737 cancer. *Semin Cancer Biol, 20*(5), 312-319. doi:
738 10.1016/j.semcancer.2010.10.001
739 Huang, T. T., & D'Andrea, A. D. (2006). Regulation of DNA repair by ubiquitylation. *Nat*
740 *Rev Mol Cell Biol, 7*(5), 323-334. doi: 10.1038/nrm1908
741 Huang, T. T., Nijman, S. M., Mirchandani, K. D., Galardy, P. J., Cohn, M. A., Haas, W.,
742 . . . D'Andrea, A. D. (2006). Regulation of monoubiquitinated PCNA by DUB
743 autocleavage. *Nat Cell Biol, 8*(4), 339-347. doi: 10.1038/ncb1378
744 J, O. W., Kawamura, K., Tada, Y., Ohmori, H., Kimura, H., Sakiyama, S., & Tagawa, M.
745 (2001). DNA polymerase kappa, implicated in spontaneous and DNA damage-
746 induced mutagenesis, is overexpressed in lung cancer. *Cancer Res, 61*(14),
747 5366-5369.
748 Johansson, E., Garg, P., & Burgers, P. M. (2004). The Pol32 subunit of DNA
749 polymerase delta contains separable domains for processive replication and
750 proliferating cell nuclear antigen (PCNA) binding. *J Biol Chem, 279*(3), 1907-
751 1915. doi: 10.1074/jbc.M310362200

752 Jones, M. J., Colnaghi, L., & Huang, T. T. (2012). Dysregulation of DNA polymerase
753 kappa recruitment to replication forks results in genomic instability. *EMBO J,*
754 *31*(4), 908-918. doi: 10.1038/emboj.2011.457
755 Kannouche, P., Broughton, B. C., Volker, M., Hanaoka, F., Mullenders, L. H., &
756 Lehmann, A. R. (2001). Domain structure, localization, and function of DNA
757 polymerase eta, defective in xeroderma pigmentosum variant cells. *Genes Dev,*
758 *15*(2), 158-172.
759 Kannouche, P. L., & Lehmann, A. R. (2004). Ubiquitination of PCNA and the
760 polymerase switch in human cells. *Cell Cycle, 3*(8), 1011-1013.
761 Kreis, N. N., Sanhaji, M., Rieger, M. A., Louwen, F., & Yuan, J. (2014). p21Waf1/Cip1
762 deficiency causes multiple mitotic defects in tumor cells. *Oncogene, 33*(50),
763 5716-5728. doi: 10.1038/onc.2013.518
764 Le Tallec, B., Koundrioukoff, S., Wilhelm, T., Letessier, A., Brison, O., & Debatisse, M.
765 (2014). Updating the mechanisms of common fragile site instability: how to
766 reconcile the different views? *Cell Mol Life Sci, 71*(23), 4489-4494. doi:
767 10.1007/s00018-014-1720-2
768 Leonhardt, H., Rahn, H. P., Weinzierl, P., Sporbert, A., Cremer, T., Zink, D., &
769 Cardoso, M. C. (2000). Dynamics of DNA replication factories in living cells. *J*
770 *Cell Biol, 149*(2), 271-280.
771 Letessier, A., Millot, G. A., Koundrioukoff, S., Lachages, A. M., Vogt, N., Hansen, R. S.,
772 . . . Debatisse, M. (2011). Cell-type-specific replication initiation programs set
773 fragility of the FRA3B fragile site. *Nature, 470*(7332), 120-123. doi:
774 10.1038/nature09745
775 Lukas, C., Savic, V., Bekker-Jensen, S., Doil, C., Neumann, B., Pedersen, R. S., . . .
776 Lukas, J. (2011). 53BP1 nuclear bodies form around DNA lesions generated by
777 mitotic transmission of chromosomes under replication stress. *Nat Cell Biol,*
778 *13*(3), 243-253. doi: 10.1038/ncb2201
779 Luzzani, C., Neiman, G., Garate, X., Questa, M., Solari, C., Fernandez Espinosa, D., . .
780 . Miriuka, S. G. (2015). A therapy-grade protocol for differentiation of pluripotent
781 stem cells into mesenchymal stem cells using platelet lysate as supplement.
782 *Stem Cell Res Ther, 6*, 6. doi: 10.1186/scrt540
783 Mansilla, S. F., Soria, G., Vallerga, M. B., Habif, M., Martinez-Lopez, W., Prives, C., &
784 Gottifredi, V. (2013). UV-triggered p21 degradation facilitates damaged-DNA
785 replication and preserves genomic stability. *Nucleic Acids Res, 41*(14), 6942-
786 6951. doi: 10.1093/nar/gkt475

787 Martin-Caballero, J., Flores, J. M., Garcia-Palencia, P., & Serrano, M. (2001). Tumor
788 susceptibility of p21(Waf1/Cip1)-deficient mice. *Cancer Res, 61*(16), 6234-
789 6238.
790 Mauro, M., Rego, M. A., Boisvert, R. A., Esashi, F., Cavallo, F., Jasin, M., & Howlett, N.
791 G. (2012). p21 promotes error-free replication-coupled DNA double-strand
792 break repair. *Nucleic Acids Res, 40*(17), 8348-8360. doi: 10.1093/nar/gks612
793 McCulloch, S. D., & Kunkel, T. A. (2008). The fidelity of DNA synthesis by eukaryotic
794 replicative and translesion synthesis polymerases. *Cell Res, 18*(1), 148-161.
795 doi: 10.1038/cr.2008.4
796 McDonald, E. R., 3rd, Wu, G. S., Waldman, T., & El-Deiry, W. S. (1996). Repair Defect
797 in p21 WAF1/CIP1 -/- human cancer cells. *Cancer Res, 56*(10), 2250-2255.
798 Minocherhomji, S., Ying, S., Bjerregaard, V. A., Bursomanno, S., Aleliunaite, A., Wu,
799 W., . . . Hickson, I. D. (2015). Replication stress activates DNA repair synthesis
800 in mitosis. *Nature, 528*(7581), 286-290. doi: 10.1038/nature16139
801 Moldovan, G. L., Pfander, B., & Jentsch, S. (2007). PCNA, the maestro of the
802 replication fork. *Cell, 129*(4), 665-679. doi: 10.1016/j.cell.2007.05.003
803 Niimi, A., Brown, S., Sabbioneda, S., Kannouche, P. L., Scott, A., Yasui, A., . . .
804 Lehmann, A. R. (2008). Regulation of proliferating cell nuclear antigen
805 ubiquitination in mammalian cells. *Proc Natl Acad Sci U S A, 105*(42), 16125-
806 16130. doi: 10.1073/pnas.0802727105
807 Nishitani, H., Shiomi, Y., Iida, H., Michishita, M., Takami, T., & Tsurimoto, T. (2008).
808 CDK inhibitor p21 is degraded by a proliferating cell nuclear antigen-coupled
809 Cul4-DDB1Cdt2 pathway during S phase and after UV irradiation. *J Biol Chem,*
810 *283*(43), 29045-29052. doi: 10.1074/jbc.M806045200
811 Noon, A. T., & Goodarzi, A. A. (2011). 53BP1-mediated DNA double strand break
812 repair: insert bad pun here. *DNA Repair (Amst), 10*(10), 1071-1076. doi:
813 10.1016/j.dnarep.2011.07.012
814 Oakley, G. G., & Patrick, S. M. (2010). Replication protein A: directing traffic at the
815 intersection of replication and repair. *Front Biosci (Landmark Ed), 15*, 883-900.
816 Ohashi, E., Bebenek, K., Matsuda, T., Feaver, W. J., Gerlach, V. L., Friedberg, E. C., .
817 . . Kunkel, T. A. (2000). Fidelity and processivity of DNA synthesis by DNA
818 polymerase kappa, the product of the human DINB1 gene. *J Biol Chem,*
819 *275*(50), 39678-39684. doi: 10.1074/jbc.M005309200
820 Ozeri-Galai, E., Bester, A. C., & Kerem, B. (2012). The complex basis underlying
821 common fragile site instability in cancer. *Trends Genet, 28*(6), 295-302. doi:
822 10.1016/j.tig.2012.02.006

823 Ozeri-Galai, E., Lebofsky, R., Rahat, A., Bester, A. C., Bensimon, A., & Kerem, B.
824 (2011). Failure of origin activation in response to fork stalling leads to
825 chromosomal instability at fragile sites. *Mol Cell, 43*(1), 122-131. doi:
826 10.1016/j.molcel.2011.05.019
827 Pillaire, M. J., Betous, R., Conti, C., Czaplicki, J., Pasero, P., Bensimon, A., . . .
828 Hoffmann, J. S. (2007). Upregulation of error-prone DNA polymerases beta and
829 kappa slows down fork progression without activating the replication
830 checkpoint. *Cell Cycle, 6*(4), 471-477.
831 Plosky, B. S., Vidal, A. E., Fernandez de Henestrosa, A. R., McLenigan, M. P.,
832 McDonald, J. P., Mead, S., & Woodgate, R. (2006). Controlling the subcellular
833 localization of DNA polymerases iota and eta via interactions with ubiquitin.
834 *EMBO J, 25*(12), 2847-2855. doi: 10.1038/sj.emboj.7601178
835 Prives, C., & Gottifredi, V. (2008). The p21 and PCNA partnership: a new twist for an
836 old plot. *Cell Cycle, 7*(24), 3840-3846.
837 Rey, L., Sidorova, J. M., Puget, N., Boudsocq, F., Biard, D. S., Monnat, R. J., Jr., . . .
838 Hoffmann, J. S. (2009). Human DNA polymerase eta is required for common
839 fragile site stability during unperturbed DNA replication. *Mol Cell Biol, 29*(12),
840 3344-3354. doi: 10.1128/MCB.00115-09
841 Savio, M., Coppa, T., Cazzalini, O., Perucca, P., Necchi, D., Nardo, T., . . . Prosperi, E.
842 (2009). Degradation of p21CDKN1A after DNA damage is independent of type
843 of lesion, and is not required for DNA repair. *DNA Repair (Amst), 8*(7), 778-785.
844 doi: 10.1016/j.dnarep.2009.02.005
845 Soria, G., & Gottifredi, V. (2010). PCNA-coupled p21 degradation after DNA damage:
846 The exception that confirms the rule? *DNA Repair (Amst), 9*(4), 358-364.
847 Soria, G., Podhajcer, O., Prives, C., & Gottifredi, V. (2006). P21Cip1/WAF1
848 downregulation is required for efficient PCNA ubiquitination after UV irradiation.
849 *Oncogene, 25*(20), 2829-2838. doi: 10.1038/sj.onc.1209315
850 Soria, G., Speroni, J., Podhajcer, O. L., Prives, C., & Gottifredi, V. (2008). p21
851 differentially regulates DNA replication and DNA-repair-associated processes
852 after UV irradiation. *J Cell Sci, 121*(Pt 19), 3271-3282. doi: 10.1242/jcs.027730
853 Sutherland, G. R., Parslow, M. I., & Baker, E. (1985). New classes of common fragile
854 sites induced by 5-azacytidine and bromodeoxyuridine. *Hum Genet, 69*(3), 233-
855 237.
856 Techer, H., Koundrioukoff, S., Carignon, S., Wilhelm, T., Millot, G. A., Lopez, B. S., . . .
857 Debatisse, M. (2016). Signaling from Mus81-Eme2-Dependent DNA Damage
858 Elicited by Chk1 Deficiency Modulates Replication Fork Speed and Origin
859 Usage. *Cell Rep, 14*(5), 1114-1127. doi: 10.1016/j.celrep.2015.12.093

Tsanov, N., Kermi, C., Coulombe, P., Van der Laan, S., Hodroj, D., & Maiorano, D. (2014). PIP degron proteins, substrates of CRL4Cdt2, and not PIP boxes, interfere with DNA polymerase eta and kappa focus formation on UV damage. *Nucleic Acids Res, 42*(6), 3692-3706. doi: 10.1093/nar/gkt1400

Vallerga, M. B., Mansilla, S. F., Federico, M. B., Bertolin, A. P., & Gottifredi, V. (2015). Rad51 recombinase prevents Mre11 nuclease-dependent degradation and excessive PrimPol-mediated elongation of nascent DNA after UV irradiation. *Proc Natl Acad Sci U S A, 112*(48), E6624-6633. doi: 10.1073/pnas.1508543112

Ward, I. M., & Chen, J. (2001). Histone H2AX is phosphorylated in an ATR-dependent manner in response to replicational stress. *J Biol Chem, 276*(51), 47759-47762. doi: 10.1074/jbc.C100569200

Warfel, N. A., & El-Deiry, W. S. (2013). p21WAF1 and tumourigenesis: 20 years after. *Curr Opin Oncol, 25*(1), 52-58. doi: 10.1097/CCO.0b013e32835b639e

Yang, W., & Woodgate, R. (2007). What a difference a decade makes: insights into translesion DNA synthesis. *Proc Natl Acad Sci U S A, 104*(40), 15591-15598. doi: 10.1073/pnas.0704219104

Zhang, Y., Yuan, F., Xin, H., Wu, X., Rajpal, D. K., Yang, D., & Wang, Z. (2000). Human DNA polymerase kappa synthesizes DNA with extraordinarily low fidelity. *Nucleic Acids Res, 28*(21), 4147-4156.

Figure titles and legends

FIGURE 1: The PCNA interacting region of p21 facilitates the recruitment of p21 to replication factories in cycling cells. A) Representative images of p21 in EdU positive and negative cells (left panel) and from U2OS cells transfected with control siRNA (siLuc) or sip21 (right panel). B) p21 intensity in the indicated samples. Nuclei were counterstained with DAPI. 70 nuclei/sample; 3 independent experiments were performed. C) Representative images from Proximity ligation assay (PLA) performed after mild extraction on the indicated samples. D) Quantification of PLA experiments described in C. 100 nuclei/sample; 2 independent experiments were performed. E) Colocalization of p21 foci with GFP-PCNA which reveal replication factories (mild extraction was applied). F) Profiles of signal intensity along an arbitrary line (showed in

E) drawn across the nuclei. G and H) Samples were transfected with the indicated p21 mutants. Representative images are shown. Samples treated or not with CSK buffer were classified into the indicated categories.100 nuclei/ sample; 2 independent experiments were analysed. For all figures in this manuscript: significance of the differences are: *p<0.1; **p<0.01; ***p<0.001. When the difference is not statistically significant, the p value is not shown. Error bars represent SEM (standard error of the mean).

FIGURE 2: The depletion of endogenous p21 impairs the choreography of unperturbed DNA replication. A) Western blot (W.B.) analysis showing p21 levels in U2OS cells transfected with the indicated siRNAs. B) EdU positive cells. 200 nuclei/sample were analysed in three independent experiments. C) The percentage of cells with CSK-resistant PCNA nuclear retention. 300 nuclei/sample were analysed in three independent experiments. D) Relative amount of cells with early or mid/late PCNA distribution. 100 nuclei/sample were examined in three independent experiments. E) Representative fibers from control (siLuc) or sip21 transfected cells. F) IdU track length. 100 fibers/samples were analysed in three independent experiments. G) Schematic representation of the different structures that can be measured in the fiber analysis. H) Samples in F were used to analyse the frequency of origin firing as the relative number of origins [(red-green-red + red only fibers)/total fibers]. 200 fibers/samples were analysed in three independent experiments.

FIGURE 3: In the absence of DNA damage, replication stress markers and genomic instability increase when p21 is depleted. A) Quantification of γ H2AX intensity in the nucleus of U2OS transfected with the indicated siRNA. 200 nuclei/sample were examined in three independent experiments. Representative images are showed in the lower part of the panel. B) U2OS cells with more than five 53BP1 foci were quantified. 200 cells/sample were analysed in three independent experiments. Representative images are showed in the lower part of the panel. C)

Quantification of cells with RPA foci. 150 nuclei positive for PCNA-resistance to CSK extraction/sample were examined in three independent experiments. D) Quantification of cells with perinuclear DNA (MN) accumulation. 300 binucleated U2OS cells/samples were inspected in three independent experiments. Representative images are shown on the right. E) Quantification of CFS expression for the indicated conditions. APH treatment corresponds to 0.2μm for 24h. 50 metaphases from HCT116 cells/sample were examined in three independent experiments.

FIGURE 4: Mechanistically distinct regulators of alt DNA pols are required to facilitate unperturbed DNA replication. A) W.B. analysis revealing PCNA, ubi-PCNA and p21 levels in U2OS cells transfected with the indicated siRNAs. B) USP1 mRNA levels were examined by quantitative RT-PCR. C) Model depicting the different mechanisms of PCNA regulation by p21 and USP1. D) IdU track length was measured in 85 fibers/sample in three independent experiments. E) Origin firing frequency. 150 fibers/sample were analysed in three independent experiments. F) Quantification of cells with more than five 53BP1 foci. 200 U2OS cells/sample were analysed in three independent experiments. G) MN accumulation. 300 binucleated cells/sample were analyzed in three independent experiments. Data on the effect of USP1 downregulation on the modulation of nascent DNA elongation (Figure 4D) and accumulation of cells with 53BP1 foci (Figure 4F) and micronuclei (Figure 4G) was reproduced from Jones et al, EMBO.

Figure 5: The recruitment of pol κ to replication-associated structures increases in the absence of p21. A) U2OS cells were transfected with GFP-polκ. Representative images of cells with and without with GFP-pol κ foci. B) Percentages of cells with GFP-pol κ focal organization. 150 nuclei/sample were analyzed in two independent experiments. C) siLuc and sip21 depleted samples were subjected to chromatin immunoprecipitation using a monoclonal PCNA antibody. GFP-pol κ recruitment to chromatin was revealed by using GFP antibodies. The result was reproduced in three

946 independent experiments. D) Proximity Ligation Assay (PLA) between PCNA and
947 endogenous pol κ was performed in U2OS cells. Two representative images of PLA in
948 siLuc and sip21 cells are shown. E) Quantification of PLA foci per nuclei. More than
949 1000 nuclei were analysed in three independent experiments.

950 **FIGURE 6: Pol κ depletion prevents the DNA replication defects and the genomic**
951 **instability caused by p21 downmodulation.** A) Western blots showing GFP-pol κ
952 and p21 levels in U2OS cells transfected with the indicated siRNAs. B) Total IdU track
953 length was evaluated in 100 fibers/sample in three independent experiments. C)
954 Frequency of origin firing. 200 fibers were analysed in three experiments. D)
955 Quantification of cells with 53BP1 foci. 200 cells were analysed in three independent
956 experiments. E) Quantification of MN accumulation. 300 binucleated cells/sample were
957 analysed in three independent experiments. F) Quantification of CFS instability in
958 HCT116 cells transfected with the indicated siRNAs. 50 metaphases/sample were
959 analysed in three independent experiments. G) Representative images of the CFS
960 analysed in F.

961 **FIGURE 7: Pol κ-mediated replication defects of p21-depleted cells are**
962 **transmitted to the M and G1 phases of the cell cycle.** A) Quantification of phospho-
963 H3 positive U2OS. 200 cells/sample were analysed in three independent experiments.
964 B) Representative images of 53BP1 bodies outside S phase. Yellow arrows indicate
965 EdU negative cells with 53BP1 foci C) Percentages of EdU negative cells which are
966 positive for 53BP1 bodies. 200 nuclei/sample were analysed in three independent
967 experiments. D) Distribution of EdU negative cells with increasing number of 53BP1
968 bodies per cell in the experiments showed in C. 100 nuclei/sample were analysed in
969 three independent experiments. E) Phospho-H3 accumulation was quantified in 200
970 nuclei/sample of three independent experiments. Samples depleted from pol κ and pol
971 η were compared. F) Percentages of cells with more than five 53BP1 foci were

determined after analysing 200 nuclei/sample in three independent experiments. Samples depleted from pol κ and pol η were compared.

FIGURE 8: The PIR domain of p21 and not the CDK-binding domain is required to prevent DNA replication defects in p21 depleted cells during unperturbed S phase. A) W.B. analysis was performed to evaluate p21 expression in U2OS cells transfected with control or p21 siRNA and infected with p21 or $p21^{PIPMut*}$ lentiviruses 6 hours later. B) Representative panel showing the efficiency of lentiviral infection (>90%). C) GFP-pol κ focal organization in samples depleted from p21 and infected with p21 or $p21^{PIPMut*}$. D) IdU track length was measured in 100 fibers/sample in three independent experiments. E) Frequency of origin firing. 100 fibers/sample were analysed in three experiments. F) Infection were performed in HCT116 p21+/+ and p21-/- cells. Representative panel showing the efficiency of lentiviral infection in HCT116 p21-/- s. G) IdU track length was measured in 100 fibers/sample in three independent experiments. H) Frequency of origin firing was measured in the experiments shown in G. 200 fibers/sample were analysed. I) Quantification of the percentage of cells with more than 5 53BP1 foci/cell. 200 cells/sample were evaluated in three independent experiments. J) Quantification of MN accumulation. 200 binucleated cells were analysed in three independent experiments.

Figure 9: p21 depletion promotes replication stress and genomic instability in primary human cells. A and B) IdU track length in Human Foreskin fibrobalsts (HFF) and Umbilical Cord Mesenchymal Stem cells (MSC). 100 fiber/sample were analysed in three independent experiments. Western blot showing p21 depletion in the indicated cell line. C) Representative fibers in siLuc and sip21 HFF cells. D) Origin frequency in HFF cells. 200 fiber/sample were analyzed in three independent experiments. E) Cells with more than 5 53BP1 foci were analyzed in MSC cells. 200 nuclei/sample were analyzed in three independent experiments. F) Representative images of 53BP1 in siLuc and sip21 MSC cells. G and H) Quantification of MN accumulation. 200

binucleated cells were analyzed in HFF and MSC cells respectively in three independent experiments. I) Representative images of Binulceated cells with and without MN.

Figure 10: Model depicting the implication of our findings. p21 levels in S phase are low but sufficient to prevent pol κ loading to replication forks. When p21 is absent, the abnormal use of pol κ during unperturbed replication impairs nascent DNA elongation. While origin firing increases to compensate the slow fork progression, late replicating and origin-poor DNA regions, i.e. CFS, are inefficiently duplicated. The replication defects accumulated in p21-depleted samples lead to genomic instability and transmission of replication defects to G1.

Figure supplements

Figure 1- figure supplement 1: **Endogenous p21 localizes to replication factories.** A) U2OS cells were not treated (NT) or UV irradiated with 20 J/m^2 and 2 hours later EdU was incorporated for 10 minutes. EdU and p21 were revealed by Click-IT technology and specific antibodies respectively. Representative panels are showed. Zoomed images correspond to the indicated yellow boxes. B) Intensity of p21 in the experiment shown in A. 50 nuclei were counted and two independent experiments were performed. C) EdU was incorporated for 10 minutes to U2OS cells. A CSK extraction buffer was used to retain only chromatin bound proteins. Endogenous p21 was revealed by immunofluorescence and the colocalization between p21 and EdU was determined generating profiles of signal intensity along an arbitrary line drawn across the nuclei. For all supplemental figures in this manuscript: significance of the differences are: *p<0.1; **p<0.01; ***p<0.001. When the difference is not statistically significant, the p value is not shown. Error bars represent SEM (standard error of the mean).

Figure 1- figure supplement 2: Chromatin bound p21 is localized at replication factories. A) The colocalization of p21 and $p21^{PIPMut*}$ to replication factories was evaluated before and after CSK extraction. While the localization of p21 to replication factories is evident in both conditions, $p21^{PIPMut*}$ does not localize to replication factories before extraction and is removed from the nuclei by CSK extraction. B) The mutation of the CDK-binding domain of p21 allows unperturbed cell cycle progression in the presence of high levels of p21. U2OS cells were transfected with the indicated expression vectors and the percentage of EdU positive cells was determined by analyzing 200 nuclei in each of the three independent experiments performed. C) Western blot of p21 and $p21^{PIPMut*}$ transfection in U2OS cells.

Figure 1- figure supplement 3: The PIR domain is required for p21 recruitment to replication factoriesU2OS cells were transfected with GFP-PCNA and p21 or $p21^{PIPMut□}$ respectively. A and C) Representative images of panuclear and foci distribution of GFP-PCNA and p21 is shown for each non-extracted condition. B and D) After pre-extraction with CSK buffer, the colocalization of p21 and PCNA was analyzed by confocal microscopy, generating profiles of signal intensity along an arbitrary line drawn across the nuclei. E) p21 and $p21^{PIPMut□}$expressing cells were subjected to CSK extraction for the indicated times. F) The p21 relative retention into the insoluble fraction was quantified by densitometric analysis. The values on the plot were normalized to the KU70 intensity for each sample.

Figure 2- figure supplement 1: Stable p21 depletion cause alterations in the DNA replication choreography of HCT116 cells. A) Whole cell extracts from isogenic HCT116 p21+/+ and HCT116 p21-/- were subjected to Western Blot analysis to verify p21 elimination. (*) represents unspecific band. B) IdU track length was measured after examining 100 fibers in three independent experiments C) Representative field

showing DNA fibers in HCT116 p21+/+ and HCT116 p21-/-.Yellow arrows indicate representative of bicolor fibers in each condition.

Figure 3 - figure supplement 1: Stable p21 depletion cause alterations in the genomic stability of HCT116 cells. A) Representative images of γH2AX intensity in HCT116 p21+/+ and p21-/- cells. B) Quantification of γH2AX intensity in HCT116 p21+/+ and p21-/- cells. 200 nuclei were counted in three independent experiments. C) Quantification of cells with more than five 53BP1 foci in HCT116 cells. 200 nuclei were counted in three independent experiments. D) Quantification of MN accumulation. 300 binucleated cells were analyzed in three independent experiments.

Figure 6- figure supplement 1: Pol κ depletion prevents the accumulation of DNA replication stress markers caused by p21 downmodulation. A) Quantification of EdU positive cells transfected with the indicated siRNAs. 200 nuclei per sample were analyzed in three independent experiments. B) Quantification of CSK-resistant, PCNA positive U2OS cells transfected with the indicated siRNAs. 250 nuclei per sample were analyzed in three independent experiments. C) Quantification of nuclei with more than 10 RPA foci in PCNA positive cells after transfection with the indicated siRNAs. 150 nuclei per sample were analyzed in three independent experiments. D) Quantification of nuclear γH2AX intensity in cells transfected with the indicated siRNAs. 200 nuclei per sample were analyzed in two independent experiments.

Figure 6- figure supplement 2: Pol κ prevents the accumulation of DNA replication stress in p21 depleted cells independently of the siRNA used and in cells stably lacking p21. A) U2OS cells were transfected with sip21 and 2 different siRNA for Pol κ. .Western Blot analysis was performed to detect endogenous p21 and

GFP- Pol κ. B) RT-PCR was performed to detect mRNA levels of p21 and Pol κ using the indicated siRNAs. C) IdU track length was measured using 2 different siRNAs for Pol κ in siLuc and sip21 depleted cells. 100fibers/sample were counted in 2 independent experiments. D) Cells with more than five 53BP1 foci were analyzed in cells depleted of p21 and using 2 different siRNAs for Pol κ. E) RT-PCR was performed in HCT116 p21+/+ and p21-/- cells to determine mRNA levels of Pol κ. F) IdU track length in HCT116 p21+/+ and p21-/- depleted of Pol κ.100fibers/sample were counted in 2 independent experiments.

Figure 6- figure supplement 3: Pol κ but not pol η depletion prevents the DNA replication defects and the genomic instability caused by p21 downmodulation. A) U2OS cells were transfected with the indicated siRNA and GFP-pol η. The percentage of cells with GFP-pol η foci was calculated after analyzing 250 nuclei in three independent experiments. B) Representative images of cells with GFP-pol η foci. C) U2OS cells were transfected with GFP-pol κ and the indicated siRNAs. Western blots were performed to detect GFP-tagged Pol κ , endogenous pol η and p21 . D) Percentage of EdU positive cells were determined with the indicated siRNA. E) DNA fiber analysis was performed in the indicated samples as described in Figure 2. The total length of the IdU track was evaluated in 100 fibers in three independent experiments. F) Samples in E were used to analyse the frequency of origins as described in Figure 2. 200 fibers were analysed in three indepedent experiments. G) Quantification of cells with more than five 53BP1 foci. 200 cells were scored in three independent experiments. H) Quantification of MN accumulation. 300 binucleated cells were scored in three independent experiments.

Figure 1

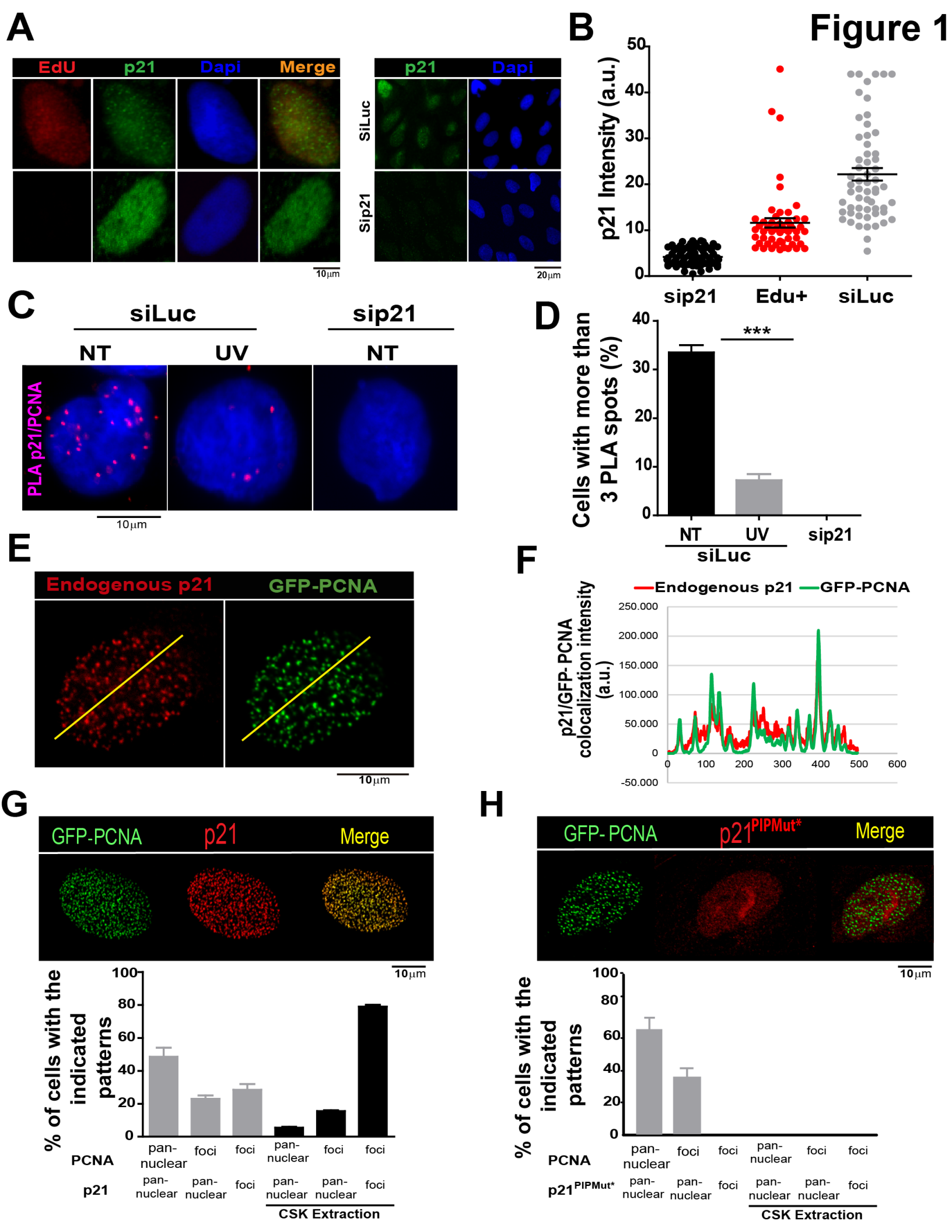
A
EdU
p21
Dapi
Merge
10µm
SiLuc
Sip21
p21
Dapi
20µm
B
p21 Intensity (a.u.)
50
40
30
20
10
0
sip21
Edu+
siLuc
C
siLuc
sip21
NT
UV
NT
PLA p21/PCNA
10µm
D
Cells with more than 3 PLA spots (%)
40
30
20
10
0
***
NT
UV
sip21
siLuc
E
Endogenous p21
GFP-PCNA
10µm
F
Endogenous p21
GFP-PCNA
p21/GFP-PCNA colocalization intensity (a.u.)
250.000
200.000
150.000
100.000
50.000
0
-50.000
0
100
200
300
400
500
600
G
GFP-PCNA
p21
Merge
10µm
% of cells with the indicated patterns
100
80
60
40
20
0
PCNA
p21
pan-nuclear
foci
foci
pan-nuclear
foci
foci
pan-nuclear
pan-nuclear
foci
pan-nuclear
pan-nuclear
foci
CSK Extraction
H
GFP-PCNA
p21PIPMut*
Merge
10µm
% of cells with the indicated patterns
100
80
60
40
20
0
PCNA
p21PIPMut*
pan-nuclear
foci
foci
pan-nuclear
foci
foci
pan-nuclear
pan-nuclear
foci
pan-nuclear
pan-nuclear
foci
CSK Extraction

Figure 2

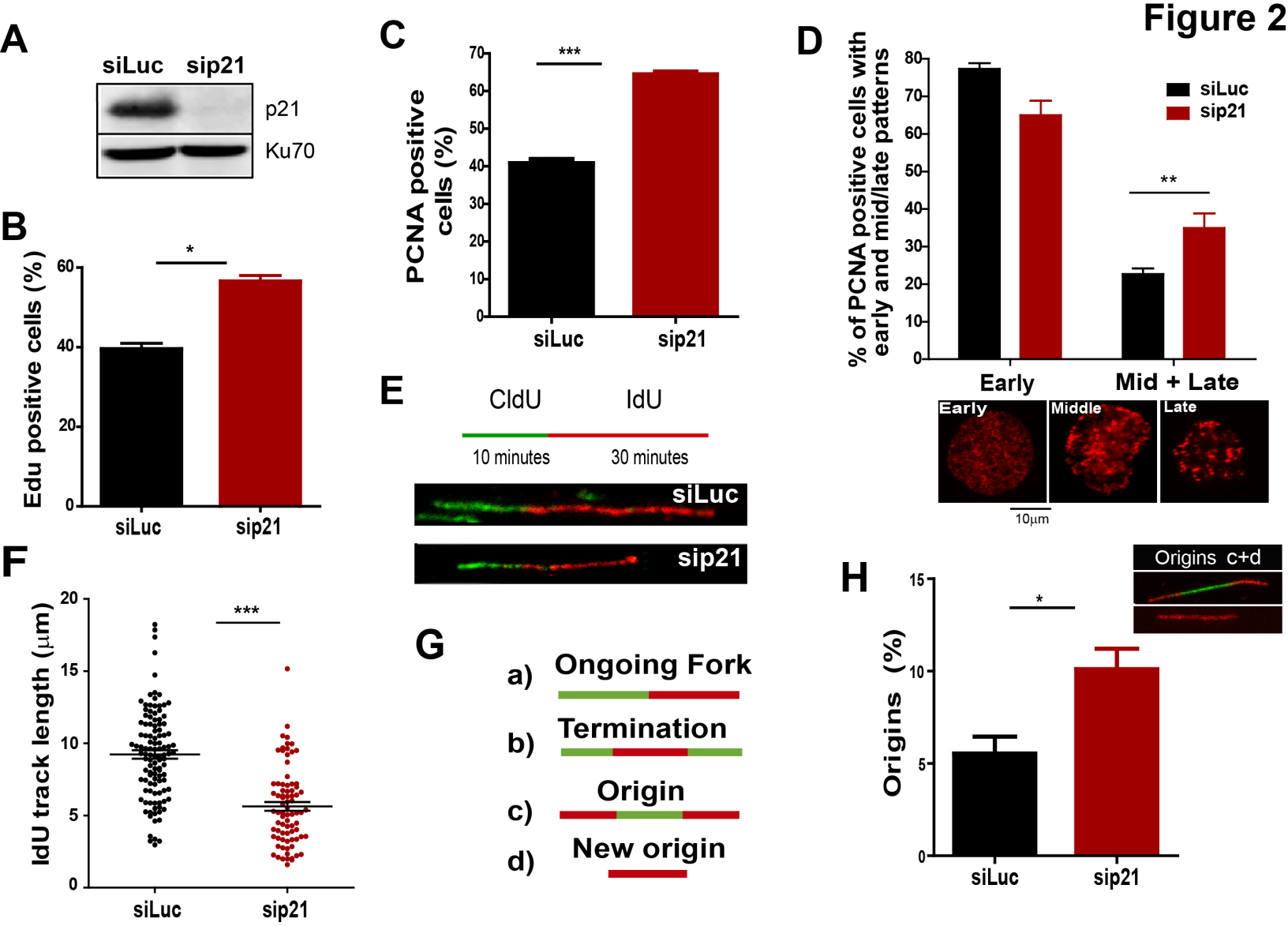
A
siLuc
sip21
p21
Ku70
B
Edu positive cells (%)
siLuc
sip21
C
PCNA positive cells (%)
siLuc
sip21
D
% of PCNA positive cells with early and mid/late patterns
siLuc
sip21
Early
Mid + Late
Early
Middle
Late
10µm
E
CldU
IdU
10 minutes
30 minutes
siLuc
sip21
F
IdU track length (µm)
siLuc
sip21
G
a) Ongoing Fork
b) Termination
c) Origin
d) New origin
H
Origins (%)
Origins c+d
siLuc
sip21

Figure 3

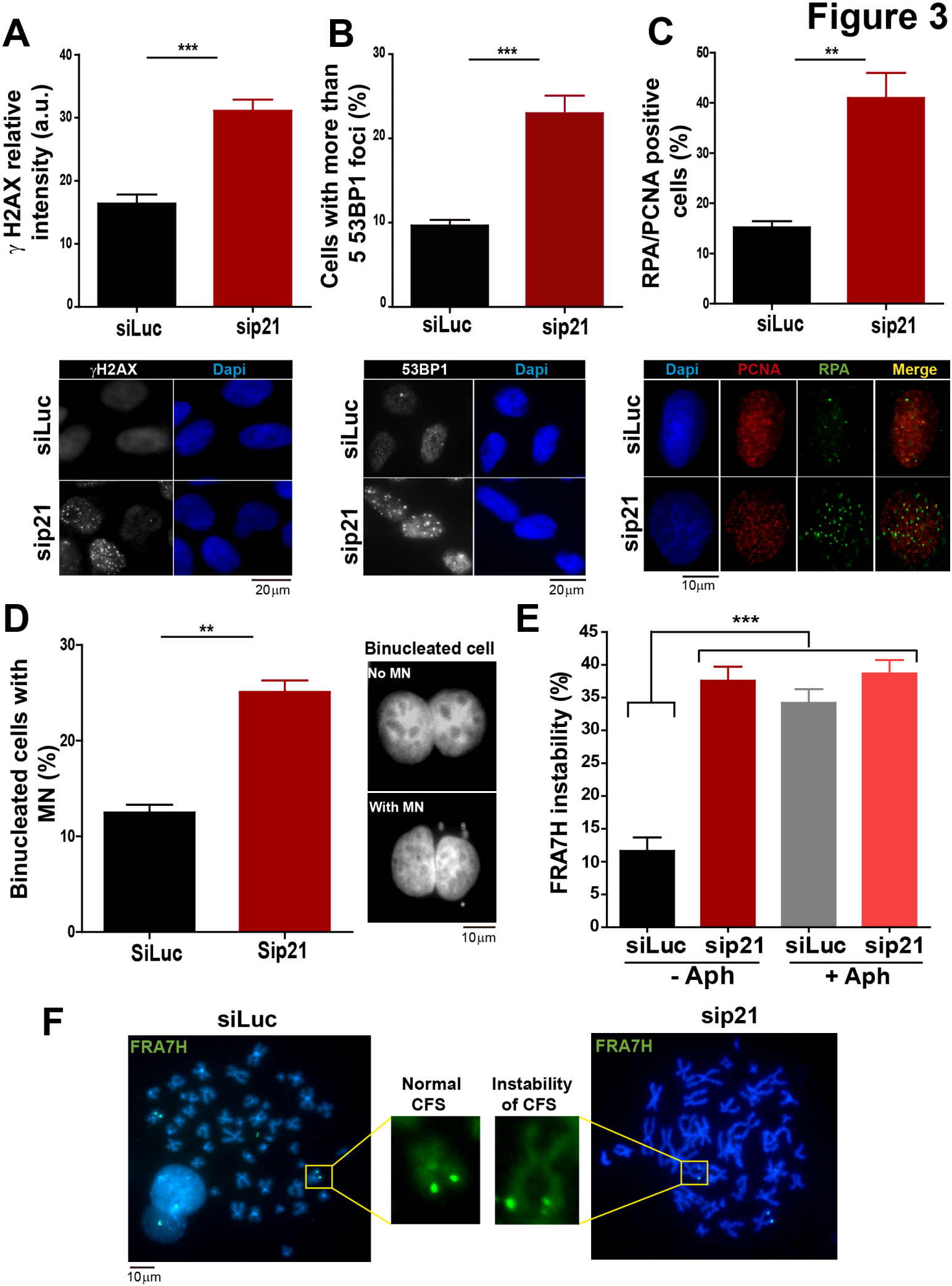
A
γ H2AX relative intensity (a.u.)
***
siLuc
sip21
B
Cells with more than 5 53BP1 foci (%)
***
siLuc
sip21
C
RPA/PCNA positive cells (%)
**
siLuc
sip21
γH2AX
Dapi
siLuc
sip21
20μm
53BP1
Dapi
siLuc
sip21
20μm
Dapi
PCNA
RPA
Merge
siLuc
sip21
10μm
D
Binucleated cells with MN (%)
**
SiLuc
Sip21
Binucleated cell
No MN
With MN
10μm
E
FRA7H instability (%)
***
siLuc
sip21
siLuc
sip21
- Aph
+ Aph
F
siLuc
FRA7H
Normal CFS
Instability of CFS
sip21
FRA7H
10μm

Figure 4

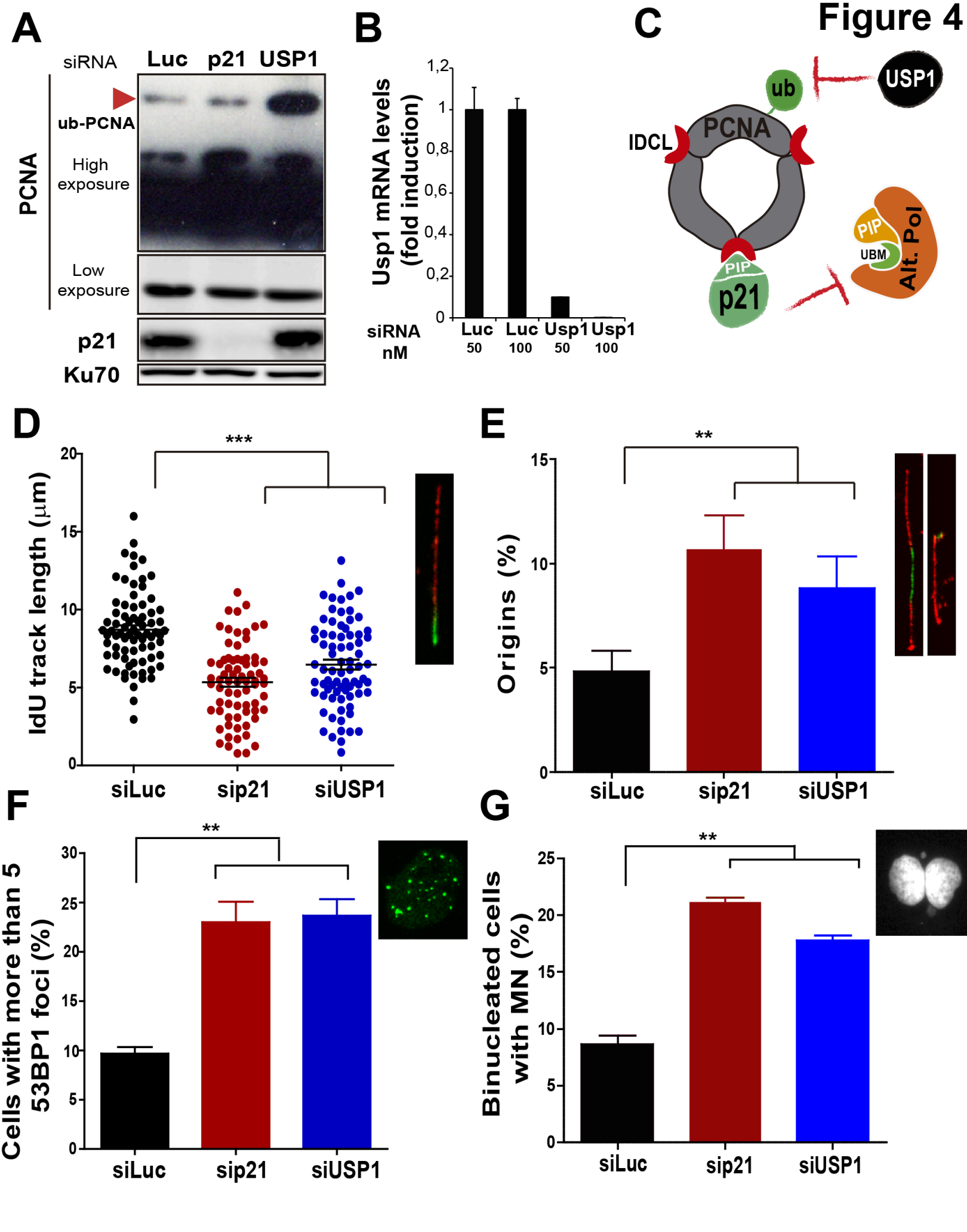
A
siRNA
Luc
p21
USP1
PCNA
ub-PCNA
High exposure
Low exposure
p21
Ku70
B
Usp1 mRNA levels (fold induction)
1,2
1
0,8
0,6
0,4
0,2
0
siRNA nM
Luc 50
Luc 100
Usp1 50
Usp1 100
C
USP1
ub
PCNA
IDCL
PIP
p21
PIP
UBM
Alt. Pol
D
***
IdU track length (μm)
20
15
10
5
0
siLuc
sip21
siUSP1
E
**
Origins (%)
15
10
5
0
siLuc
sip21
siUSP1
F
**
Cells with more than 5 53BP1 foci (%)
30
25
20
15
10
5
0
siLuc
sip21
siUSP1
G
**
Binucleated cells with MN (%)
25
20
15
10
5
0
siLuc
sip21
siUSP1

Figure 5

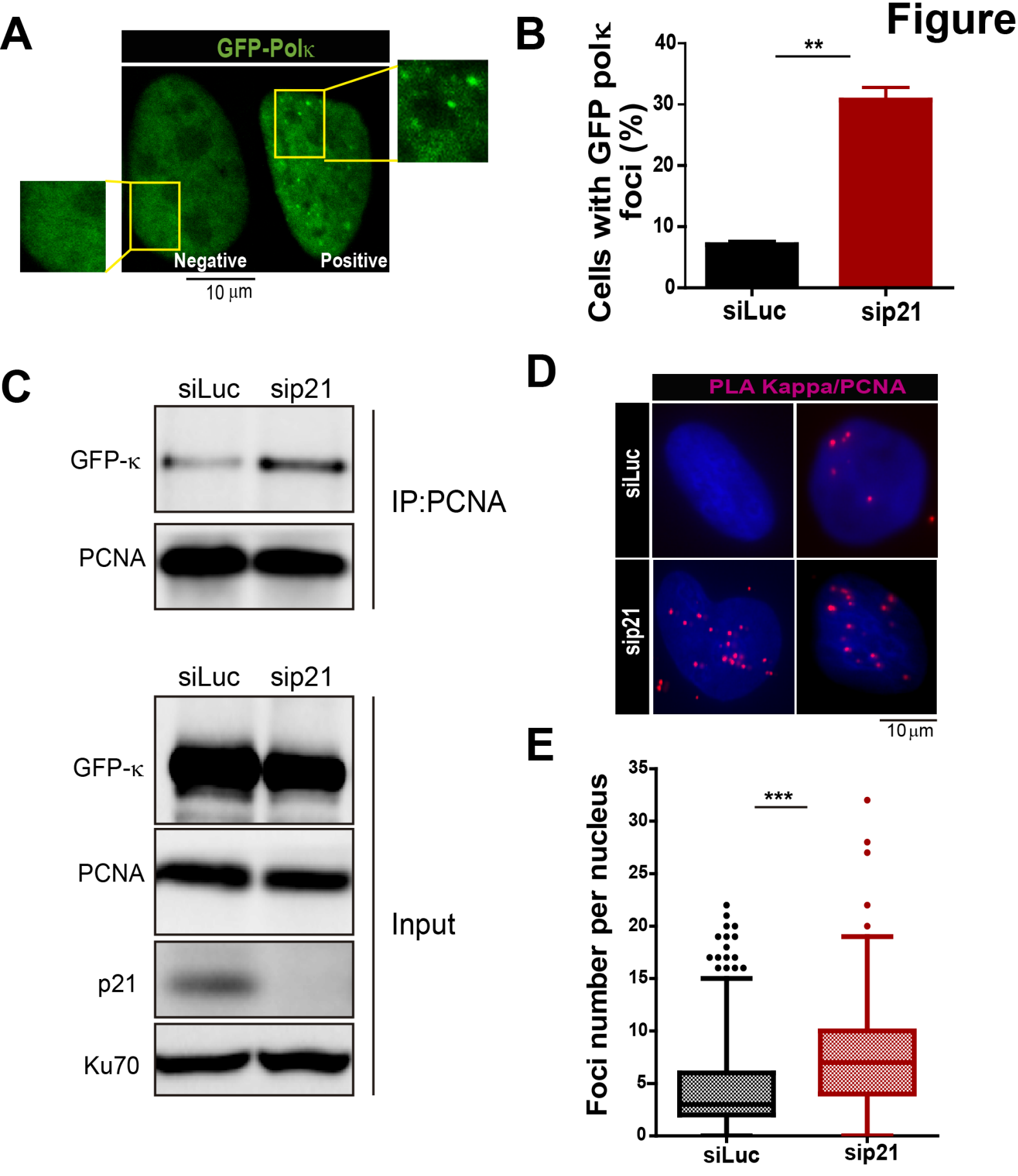
A
GFP-Polκ
Negative
Positive
10 μm
B
Cells with GFP polκ foci (%)
40
30
20
10
0
**
siLuc
sip21
C
siLuc
sip21
GFP-κ
PCNA
IP:PCNA
siLuc
sip21
GFP-κ
PCNA
p21
Ku70
Input
D
PLA Kappa/PCNA
siLuc
sip21
10 μm
E
Foci number per nucleus
35
30
25
20
15
10
5
0
***
siLuc
sip21

Figure 6

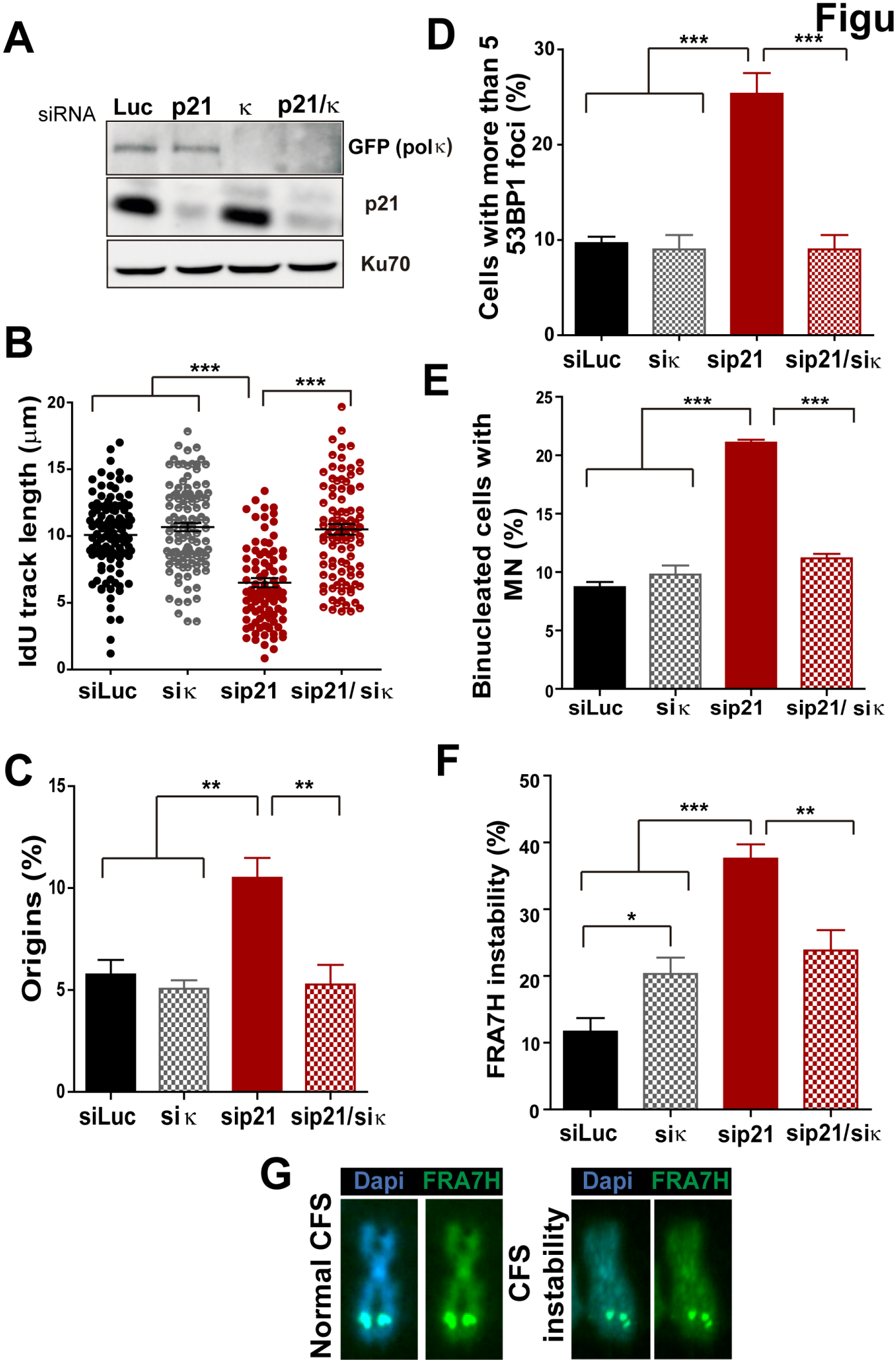
A
siRNA
Luc
p21
κ
p21/κ
GFP (polκ)
p21
Ku70
B
IdU track length (μm)
***
***
siLuc
siκ
sip21
sip21/ siκ
C
Origins (%)
**
**
siLuc
siκ
sip21
sip21/siκ
D
Cells with more than 5 53BP1 foci (%)
***
***
siLuc
siκ
sip21
sip21/siκ
E
Binucleated cells with MN (%)
***
***
siLuc
siκ
sip21
sip21/ siκ
F
FRA7H instability (%)
***
**
*
siLuc
siκ
sip21
sip21/siκ
G
Dapi
FRA7H
Normal CFS
Dapi
FRA7H
CFS instability

Figure 7

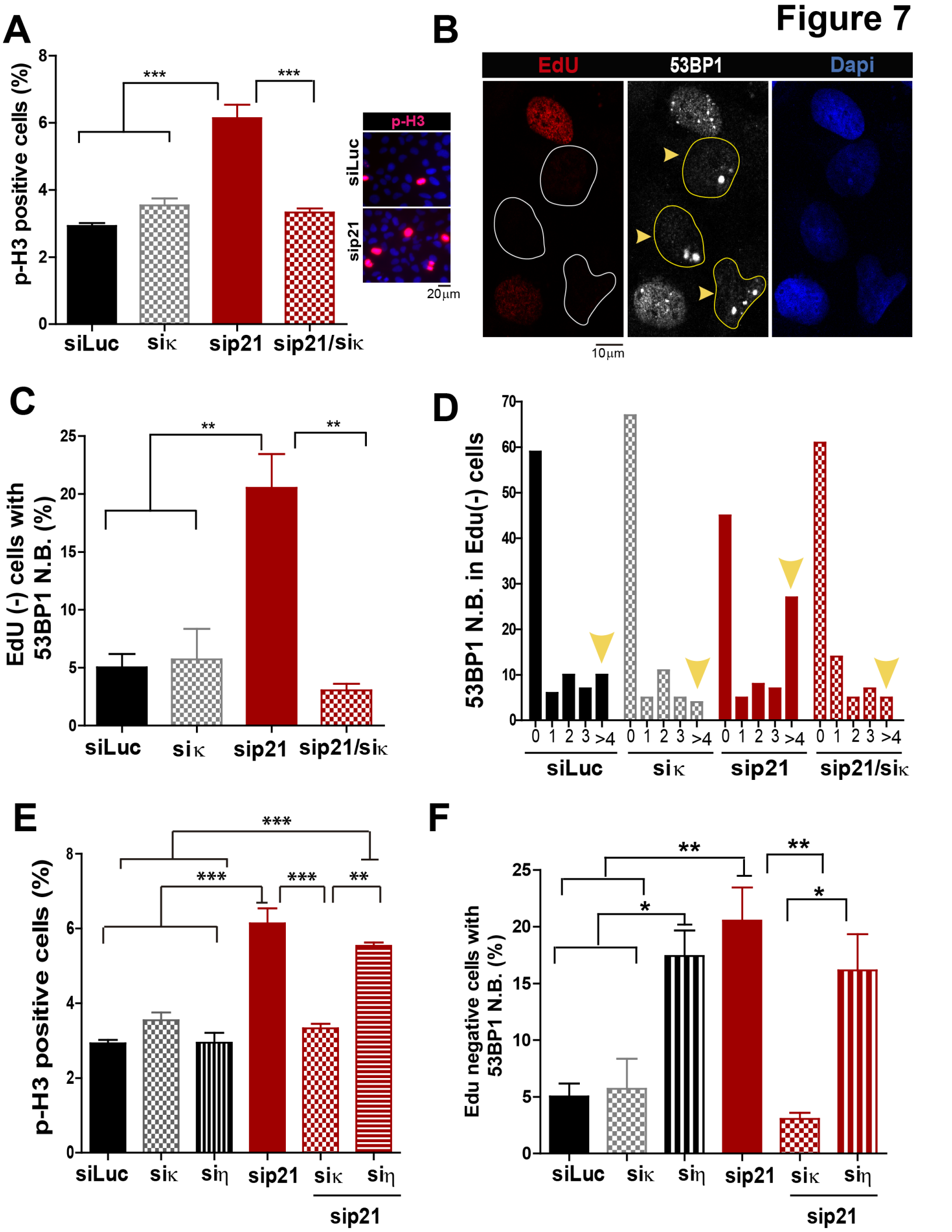
A
p-H3 positive cells (%)
***
***
p-H3
siLuc
sip21
20µm
siLuc
siκ
sip21
sip21/siκ
B
EdU
53BP1
Dapi
10µm
C
EdU (-) cells with 53BP1 N.B. (%)
**
**
siLuc
siκ
sip21
sip21/siκ
D
53BP1 N.B. in Edu(-) cells
0 1 2 3 >4
siLuc
siκ
sip21
sip21/siκ
E
p-H3 positive cells (%)
***
***
***
**
siLuc
siκ
siη
sip21
siκ
siη
sip21
F
Edu negative cells with 53BP1 N.B. (%)
**
**
*
*
siLuc
siκ
siη
sip21
siκ
siη
sip21

Figure 8

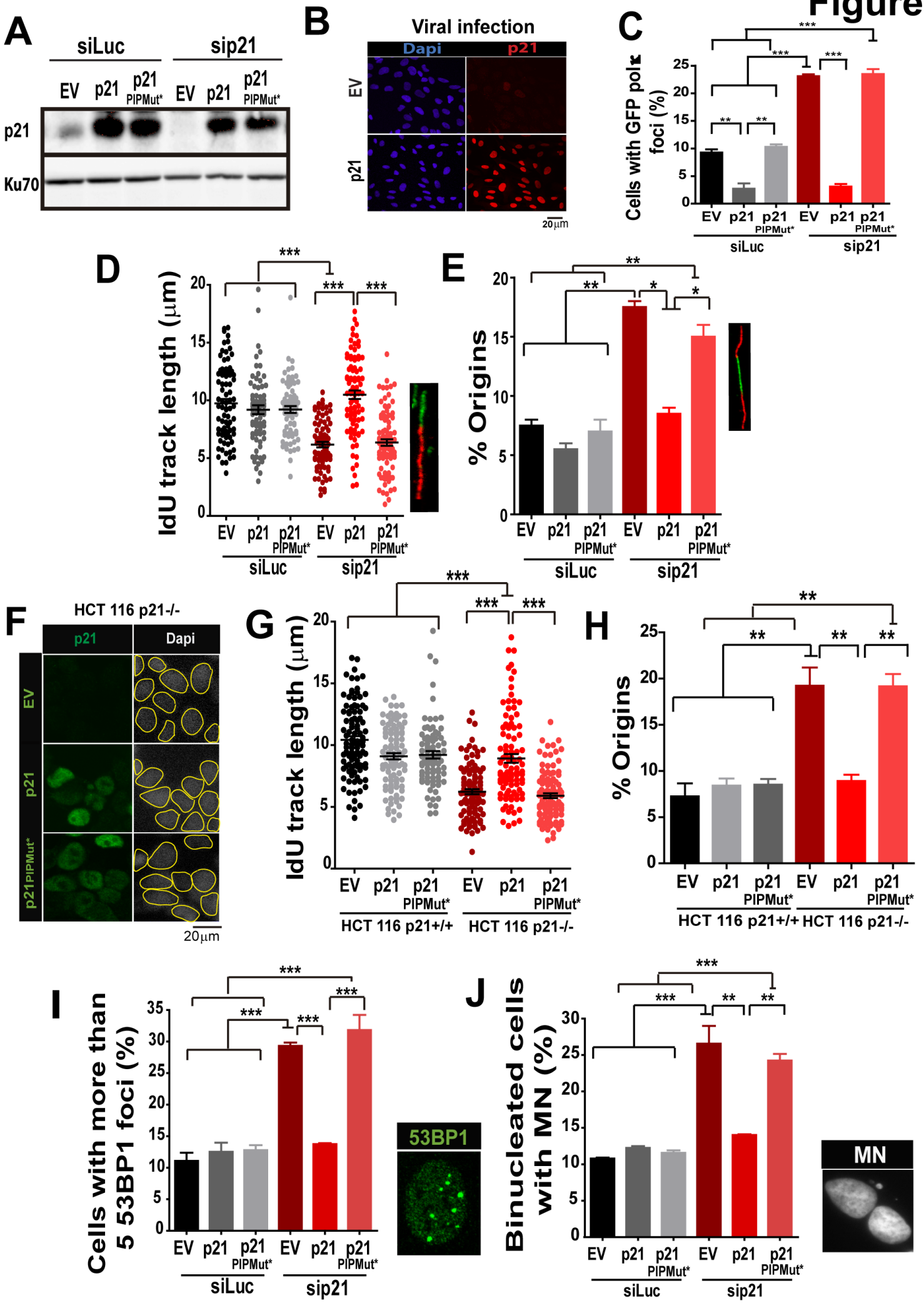
A
siLuc
sip21
EV
p21
p21 PIPMut*
p21
Ku70
B
Viral infection
Dapi
p21
EV
p21
20µm
C
Cells with GFP pol foci (%)
siLuc
sip21
D
IdU track length (µm)
E
% Origins
F
HCT 116 p21-/-
p21
Dapi
EV
p21
p21 PIPMut*
20µm
G
IdU track length (µm)
HCT 116 p21+/+
HCT 116 p21-/-
H
% Origins
I
Cells with more than 5 53BP1 foci (%)
53BP1
J
Binucleated cells with MN (%)
MN

Figure 9

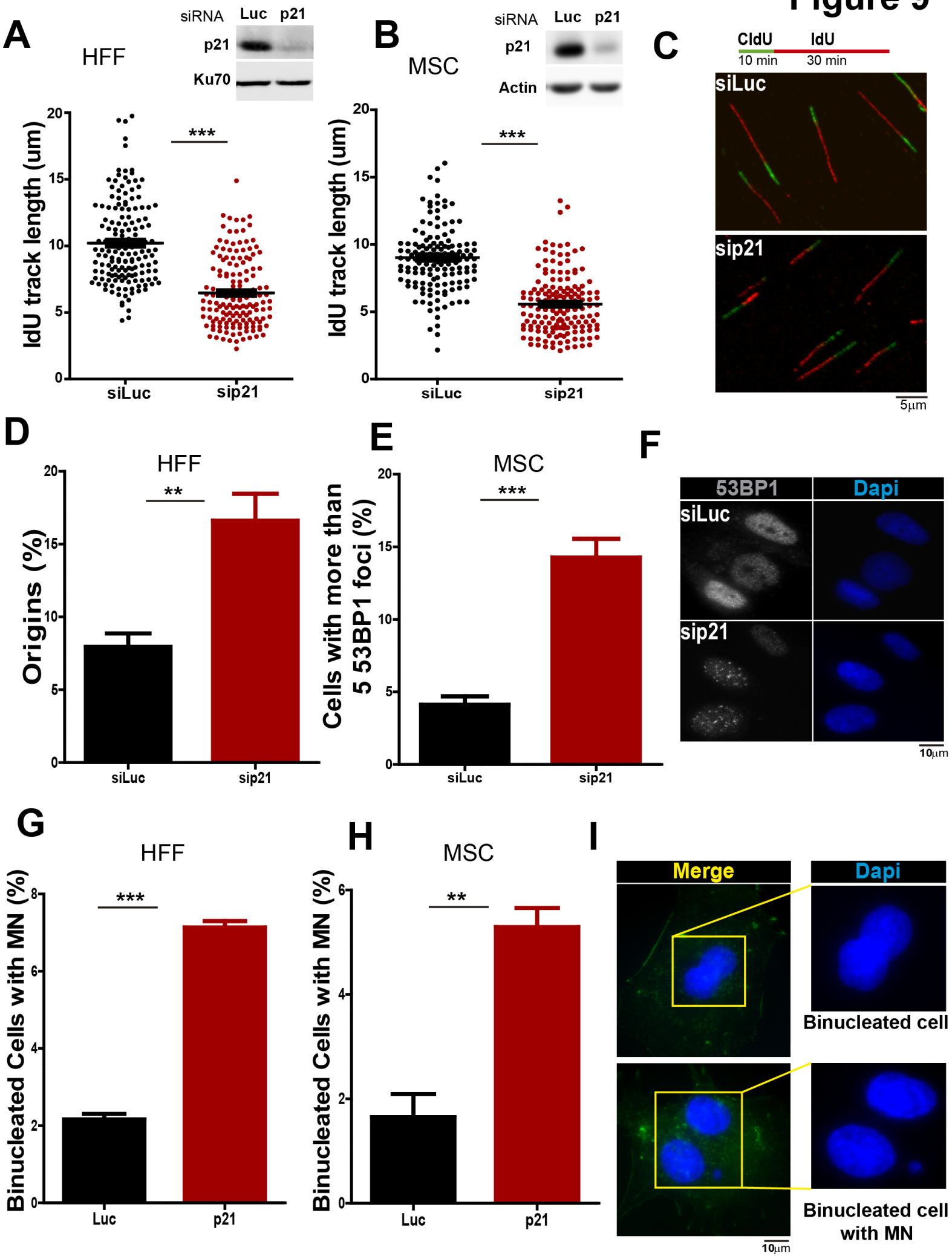
A
HFF
siRNA
Luc
p21
p21
Ku70
IdU track length (um)
***
siLuc
sip21
B
MSC
siRNA
Luc
p21
p21
Actin
IdU track length (um)
***
siLuc
sip21
C
CldU
IdU
10 min
30 min
siLuc
sip21
5µm
D
HFF
**
Origins (%)
siLuc
sip21
E
MSC
***
Cells with more than 5 53BP1 foci (%)
siLuc
sip21
F
53BP1
Dapi
siLuc
sip21
10µm
G
HFF
***
Binucleated Cells with MN (%)
Luc
p21
H
MSC
**
Binucleated Cells with MN (%)
Luc
p21
I
Merge
Dapi
Binucleated cell
Binucleated cell with MN
10µm

Figure 10

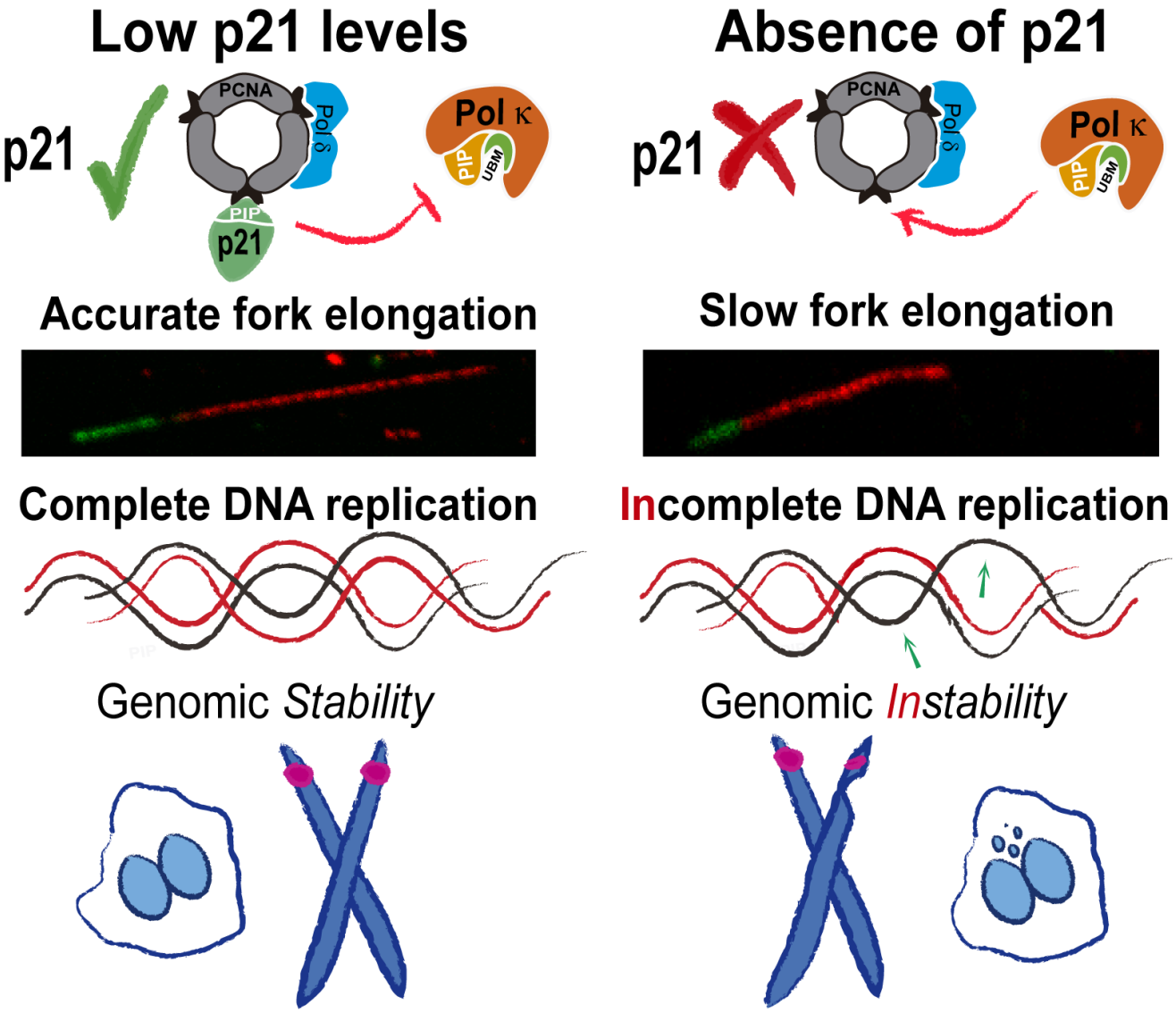
Low p21 levels
p21
PCNA
Pol δ
PIP
p21
Pol κ
PIP
UBM
Absence of p21
p21
PCNA
Pol δ
Pol κ
PIP
UBM
Accurate fork elongation
Slow fork elongation
Complete DNA replication
Incomplete DNA replication
Genomic Stability
Genomic Instability